Received: 14 September 2022 | Revised: 2 March 2023 | Accepted: 31 March 2023

DOI: 10.1002/cta.3629

WILEY

ORIGINAL PAPER

A novel hybrid image processing-based reconfiguration with RBF neural network MPPT approach for improving global maximum power and effective tracking of PV system

Chepuri Venkateswara Rao | **Rayappa David Amar Raj** | **Kanasottu Anil Naik**

Department of Electrical Engineering, National Institute of Technology, Warangal, 506004, India

Correspondence
Chepuri Venkateswara Rao, Department of Electrical Engineering, National Institute of Technology, Warangal 506004, India.
Email: venkateswararao.chepuri@gmail.com

Summary

The solar photovoltaic (PV) array output is reduced significantly by the frequently occurring inevitable partial shading conditions. In consequence, the array exhibits multiple peaks in its characteristics that cause the conventional maximum power point tracking (MPPT) algorithms to get stuck at the local maximum. So, to track the global maximum power (GMP) among the multiple peaks, a novel radial basis function (RBF)-based neural network approach has been proposed for predicting the optimal GMP. Additionally, a novel and intelligent encryption-based ruler transform (RT) reconfiguration approach is proposed to disperse the shading effect enhancing the GMP and mitigating the multiple peaks. The effectiveness of the proposed RBF-MPPT and novel RT-reconfiguration strategies has been tested and analyzed for a 5×7 PV array under distinct dynamic, uniform, and nonuniform shading conditions. The results of the proposed RBF have been compared with the conventional incremental conductance (INC) algorithm before and after reconfiguration of the PV array. Further, the ease of GMP tracking by a simple conventional INC due to the reduction of peaks after the array reconfiguration under shading conditions has been demonstrated and discussed in detail. After reconfiguration, the GMP is enhanced by 37.35%, 31.41%, 30.86%, 21.46%, 13.69%, and 8.88%, using the proposed RBF for the considered five shading conditions. The steady-state oscillations are also considerably mitigated by employing the proposed reconfiguration and RBF strategies.

KEYWORDS

encryption, global maximum power, multiple peaks, partial shading, radial basis function, reconfiguration

1 | INTRODUCTION

The adoption of sustainable advancement and circular economy solutions has become crucial due to the depletion of fossil fuels and the serious ecological problems. Globally widespread concerns that are in line with the principles of the "green economy" have been raised, in particular, about the development and usage of diverse renewable energy sources. Due to its clear advantages, such as easy deployment, high safety, no or little maintenance, and environmental friendliness, solar energy has recently attained the most widespread usage among different renewable energy sources.[1]

The reliable and quick extraction of the maximum power from the solar PV arrays under a variety of environmental conditions is typically a crucial function of the maximum power point tracking (MPPT) systems.[2] Nearly all MPPT algorithms can, by a considerable margin, achieve proper functioning for PV systems with constant solar irradiation. However, under the partial shadowing (PS) condition, the power versus voltage characteristics becomes very nonlinear exhibiting several local maximum power peaks (LMPPs). This makes the global maximum power (GMP) tracking among multiple LMPPs quite challenging.[3] The PS conditions can very easily lead to power losses, hot-spots formation effects, and problems related to the safety and reliability of PV systems. To address such issues, numerous strategies have been devised to successfully implement the GMP tracking of PV systems during PS conditions.

In general, the MPPT-based strategies are classified into conventional, soft-computing, hybrid, and other advanced strategies. The conventional strategies include perturb and observe, incremental conductance (INC), and hill-climbing algorithms.[4] Since there exists only one power peak that varies with solar irradiation or temperature, the conventional MPPT algorithms can typically achieve satisfactory MPPT performance under uniform conditions. All of the aforementioned algorithms oscillate continuously around the GMP, and this could result in power losses. Additionally, traditional MPPT algorithms have demonstrated poor GMP tracking performance under PS. Despite their compromising performance, they are being widely used for various commercial applications of PV systems due to their cost effectiveness and ease of implementation. Therefore, the soft-computing and other advanced strategies are to be employed to track the GMP accurately with minimal oscillations.

The soft-computing strategies include metaheuristic algorithms, hybrid algorithms, fuzzy logic control, and artificial neural networks (ANNs). In recent days, various metaheuristic optimization algorithms such as honey badger algorithm,[5] collaborative swarm algorithm (CSA),[6] particle swarm optimization (PSO),[6] ant colony-based new pheromone update (ACO-NPU), JAYA algorithm,[7] grey wolf optimizer (GWO),[8] logarithmic PSO (LPSO),[9] and pigeon-inspired optimization[10] have been employed to determine the GMP under PS. All these algorithms can efficiently determine GMP additionally mitigating the steady-state oscillations. Further, a vast search is achievable, handling nonlinearity and works under rapid irradiation variations. However, they inherit numerous drawbacks such as gigantic computation procedures, parameter initialization challenges, increased computational burden and tracking time, convergence issues if the GMP lies beyond the search zone, difficulty in achieving the trade-off between local exploitation & global exploration, and high randomness.

The hybrid-MPPT algorithms[11,12] can usually perform quite adequate results under PS, which owns the merits of each algorithm. Nevertheless, their design is more complex than the individual; hence, the computational burden is considerably larger. Besides, how to choose the appropriate algorithms (e.g., number or type) for combination stays unresolved. Recently, the fuzzy logic rule-based computing MPPT techniques,[13,14] where a look-up table is developed to decrease the error in the control variables, are proposed. These strategies don't necessitate knowledge of the precise model. Nevertheless, they involve a complex design, complicated hardware execution usually requiring a DSP processor, and rule declaration difficulties. Additionally, the design of the rule table only relies on the programmer's experience requiring periodic tuning. To create appropriate membership functions, the designer must have a solid understanding of PV system operation.

The biological neural network, which in essence integrates various parameters to certain data points, is reflected in ANN. To integrate diverse parameters, ANN models don't require a mathematical equation or a complicated mathematical background. In order to correlate multiple parameters with enormous amounts of unknowable data points, ANN requires minimal theoretical study than traditional approaches.[15] It is employed to train and assess a PV system's I-V and P-V nonlinearity relation. To optimize the behavior of the solar power system for maximum power, ANN continuously learns from inputs including input current and voltage, temperature, irradiance, and atmospheric data. The merits of ANN comprise exceptionally precise modeling of nonlinearity and problem-solving without requiring prior knowledge of models.[16] The input information is held in its networks rather than in the database. Therefore, the information loss does not impact its operation. The network may still identify the error and provide the output irrespective of whether the neuron does not react or data is lost. Neural networks can carry out multiple tasks simultaneously without affecting the system's performance. They have the potential to learn from faults hence improving their ability to execute competently. Employing them in the solar PV systems, the ANN-based MPPT techniques[15,16] react faster to real-time varying environments, extracting the GMP with fewer oscillations close to the GMP with minimal transient time.

Despite the recent advancements and vast investigations on improving the MPPT efficiency, tracking the GMP among the numerous power peaks remains challenging. Hence, mitigating the LMPPs by equalizing the irradiation between the rows of the PV array through an efficient and intelligent reconfiguration process solves the problem to a

maximum extent.[17] Reconfiguring the PV array not only mitigates the LMPPs but also enhances the GMP by a significant percentage due to the reduction in the mismatch. The recent developments and the existing research on various static and dynamic reconfiguration strategies have been reviewed in detail in Yang et al.[18] The dynamic reconfiguration strategies encompass various optimization based,[19–22] electrical array reconfiguration (EAR) based,[23,24] artificial intelligence (AI) based,[25,26] adaptive array reconfiguration based,[27] and so forth. Further, the static strategies include puzzle-based,[28] chaotic-based,[29] magic square-based,[30] logic-based,[31] and analytical[32] and shift-based[33] strategies. The static reconfiguration strategies are preferred over the dynamic ones due to their practical and economic feasibility issues. However, the majority of these static reconfiguration techniques currently in use have several shortcomings such as scalability and compatibility issues, nonuniform shade dispersion, inconsistency, and exhibiting numerous power peaks, which call for further research and improvement. The uniform dispersal of shade through efficient reconfiguration smoothens the array characteristics by mitigating the LMPPs and further improves the GMP. So, an intelligent reconfiguration strategy inspired by the concept of encryption has been proposed to maximize the extraction of GMP and result in accurate tracking with negligible oscillations.

Almost all the existing works on array reconfiguration strategies and MPPT algorithms have been explored separately by researchers up to date. Hardly there is no exploration or good research work on demonstrating the combined advantages/benefits of employing both reconfiguration and MPPT strategies together. Hence, in this paper, the authors proposed a novel hybrid image processing-based reconfiguration with an RBF neural network MPPT approach for enhancing the global maximum power and effective tracking of the PV system. The novelty and main contributions of the paper are as follows:

- For the first time, a hybrid reconfiguration and MPPT approach has been proposed to enhance and track the GMP effectively.
- Contrary to contemporary approaches that disperse the shade randomly, the proposed encryption-based ruler transform (RT) reconfiguration approach intelligently disperses the shade mitigating the correlation between adjoining shaded panels in row, diagonal, and column-wise directions equalizing the irradiation and mitigating the mismatch and LMPPs.
- A vast majority of the reconfiguration algorithms are applicable to only symmetrical PV array sizing. Further, the existing ones, despite being scalable to most symmetrical arrays, exhibit nonuniform shade dispersion and inconsistency. Hence, to validate the scalability and consistent superiority of the proposed reconfiguration algorithm for practical array sizes, a 5×7 PV array has been considered for the analysis.
- A novel radial basis function (RBF)-based neural network approach to predict the corresponding duty ratio of the optimal GMP resulting in negligible oscillations around GMP under partial shading conditions has been developed.
- The proposed RBF-based MPPT approach has been extensively studied under various uniform dynamic shadings cases (such as Ropp irradiance, sine irradiance, and constant irradiance profiles) and five distinct nonuniform shading conditions.
- The performance of the proposed RBF has been compared with the conventional INC-based MPPT under distinct considered shading conditions.
- Further, the ease and simplicity of tracking the GMP of the reconfigured PV array (without being stuck at LMPP) by the conventional INC under partial shading conditions have been demonstrated and discussed in detail.
- The comparative analysis of the various performance metrics of the studied MPPT approaches under PS conditions with and without reconfiguration has been presented.

The organization of the paper is as follows: Section 1 details the introduction. Section 2 details the mathematical modeling of the PV system. The detailed procedure of the proposed methodology is explained in Section 3. The MATLAB simulation results of the proposed methodology are provided in Section 4. Section 5 concludes the paper.

2 | MATHEMATICAL MODELING OF SOLAR PV SYSTEM

The PV system majorly comprises PV array, boost converter, MPPT controller, and load. The following subsections discuss the modeling of these components.

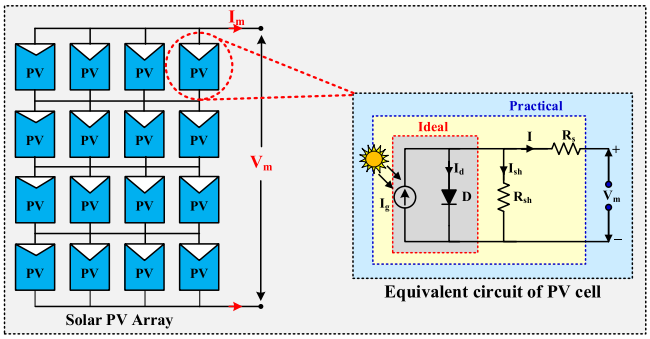

FIGURE 1 Equivalent circuit of PV cell.

2.1 | Modeling of solar PV Array

This section introduces the PV panel's mathematical formula that can be represented by the one-diode model as shown in Figure 1. Due to its simplicity, it is the widely used representation of the physical behavior of a PV panel.[34]

The current law can be used to determine the panel's output current that is obtained as follows:

$$I = I_g - I_0\left[\exp\left(q\frac{(V_m + IR_s)}{aKT}\right) - 1\right] - \left[\frac{V_m + IR_s}{R_{sh}}\right] \tag{1}$$

where q is the electron charge, a is the ideality factor of the diode, V_m is the module terminal voltage, K is the Boltzmann constant, and R_s and R_{sh} are the respective series and shunt resistances of the panel. I_g and I_o stand for the photon-generated current and reverse saturation current, respectively.[35] The amount of irradiation that reaches the panel surface determines the value of I_g, which fluctuates in accordance with the following formula:

$$I_g = I_{sc0}\left(\frac{G}{G_0}\right)(1 + \beta_i(T - T_0))\left(\frac{R_s + R_{sh}}{R_{sh}}\right) \tag{2}$$

where G is the actual incoming irradiation, β_i is the temperature coefficient of panel current, and I_{sc0} is the panel's short-circuit current at $G_0 = 1000\ \mathrm{W/m^2}$ and $T_0 = 25°\mathrm{C}$. Partial shading causes the value of radiation to fall below G_0, which leads to multiple LMPPs and a GMP peak.

2.2 | Modeling of boost converter

Boost converters are used to produce high continuous output voltages depending on the requirement.[36] The input voltage is increased to a specified level using a power electronic switch. The inductor, capacitor, switch, and diode are the four major components of a boost converter, as depicted in Figure 10. Whenever the switch is activated, the diode becomes reverse biased, the current increases, and the load is supported by an inductor and switch. Whenever the switch is turned off, the diode gets forward biased, and the current begins to discharge from the inductor, passes through the capacitor to the load, and so forth. The boost converter is modeled as follows,[36] where V_o and V_i, respectively, are the input and output voltages, and D indicates the duty cycle given to the converter. The inductance of the boost converter, L_b, is calculated as

$$L_b = \frac{V_{in}(V_0 - V_{in})}{\Delta I * V_0 * f_{sw}} = \frac{131.5(300 - 131.5)}{2.6635 \times 300 \times 5000} = 5.55\,\mathrm{mH}$$

The capacitance of the boost converter, C_b, is calculated as

$$C_b = \frac{I_0(V_0 - V_{in})}{\Delta V * V_0 * f_{sw}} = \frac{23.35(300 - 131.5)}{3 \times 300 \times 5000} = 874.32\,\mu F$$

where V_{in} and V_o are the input and output voltages of boost converter, I_o is output current, ΔI and ΔV are the permissible current and voltage limits, and f_{sw} is the switching frequency.

2.3 | Incremental conductance MPPT algorithm

The conventional INC algorithm finds the slope of power–voltage characteristics where the GMP is tracked by scanning its peak.[37] INC algorithm employs the instantaneous conductance I/V and INC dI/dV for tracking GMP. The INC algorithm finds out the PV module's operating point on the P-V characteristics using these two data. The Equation (3) represents the operation of PV module at the GMP and Equation (4) represents the operation of PV module at the leftwards of the GMP, whereas Equation (5) represents the operation at the rightwards of GMP in the power–voltage characteristics.[37]

$$\frac{dI}{dV} = -\frac{I}{V} \qquad At\ GMP \tag{3}$$

$$\frac{dI}{dV} > -\frac{I}{V} \qquad Left\ of\ GMP \tag{4}$$

$$\frac{dI}{dV} < -\frac{I}{V} \qquad Right\ of\ GMP \tag{5}$$

The aforementioned equations are derived from the concept that the P-V characteristics at GMP has a slope of zero, as given in Equation (6)

$$\frac{dP}{dV} = 0; \quad At\ GMP \tag{6}$$

By rewriting Equation (6), the following equations are obtained:

$$\frac{dP}{dV} = I\frac{dV}{dV} + V\frac{dI}{dV} \tag{7}$$

$$\frac{dP}{dV} = I + V\frac{dI}{dV} \tag{8}$$

$$I + V\frac{dI}{dV} = 0 \tag{9}$$

The GMP is tracked using Equation (9) in the conventional INC approach, and the algorithm's flowchart is depicted in Figure 2. The INC MPPT controller senses the voltage and current of the PV module. The duty ratio of the boost converter has to be reduced if Equation (4) is satisfied, and vice versa if Equation (5) is satisfied. If Equation (9) is satisfied, the duty cycle remains unchanged.

3 | PROPOSED METHODOLOGY

The ruler sequence also referred to as the Gros sequence or the ruler function is a conventional infinite integer series formed through a recursive duplication procedure.[38] For $n = 1, 2, 3, 4, \ldots$, this sequence is typically described as the

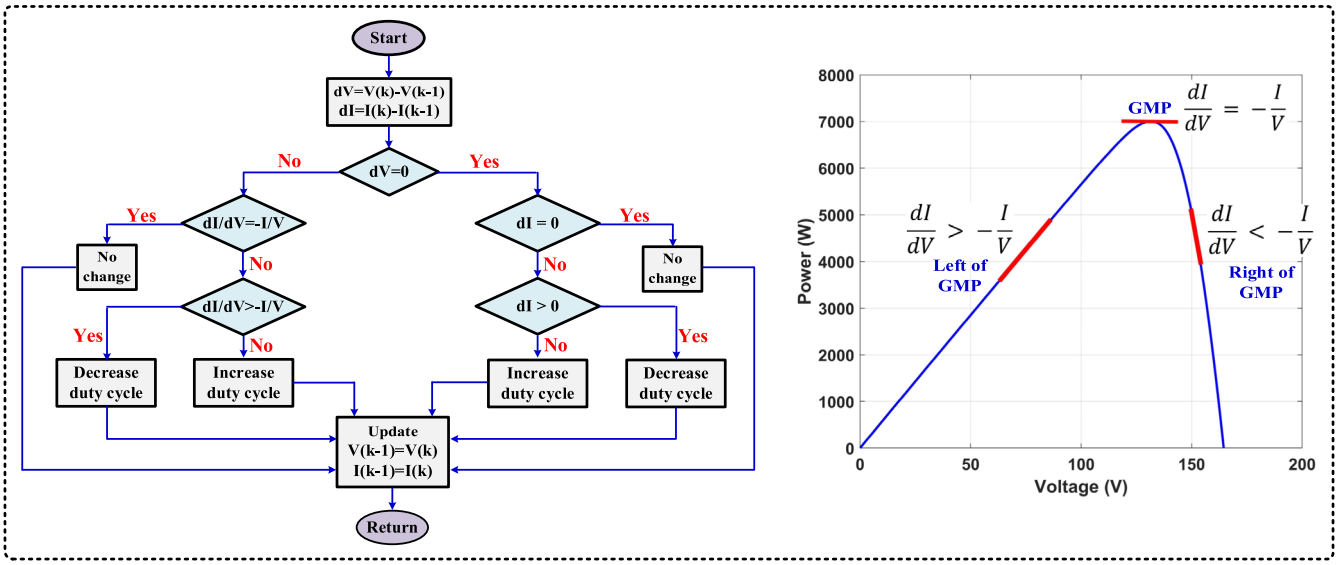

FIGURE 2 Flowchart of conventional INC-MPPT algorithm.

infinite integer series whose n^{th} term, $a(n)$, is to be the greatest power of 2 that divides $2n$. The successive terms of the sequence are as follows: {1, 2, 1, 3, 1, 2, 1, 4, 1, 2, 1, 3, 1, 2, 1, 5, 1, ...}.

3.1 | Classical description of ruler sequence

The sequence $\sigma^{(m)} = \sigma^{(m)}(1), \sigma^{(m)}(2), \sigma^{(m)}(3), \sigma^{(m)}(4), \ldots$, yielding the lengths of the glue strings $S_n^{(m)}$, appears to be a ruler sequence because $\sigma^{(m)}(n)$ effectively relies solely on the $(m+1)$-adic valuation of n.[37] If m and n are positive integers, then the highest power of m divided by n is the m-adic valuation of n, $|n|_m$. The series given by $r = r(1), r(2), r(3), r(4), \ldots$, is regarded as the standard example of a ruler sequence.

$$r(n) = |n|_2 + 1$$

Thus, the consecutive terms of the ruler sequence can be obtained as given in (10), where the bolded new record entries occur at powers of 2. The authors sometimes use Thomae's function and the ruler sequence identically.[39] In fact, the ruler sequence can be regarded as a limitation of Thomae's function to the dyadic rationals, or rational numbers with denominators that are powers of two. After a linear translation, the order of the exponents of the image of the set of dyadic rationals by h, sorted from smallest to largest, coincides with the ruler sequence if the function is defined[39] as follows:

$$h(x) = \begin{cases} 2^{-k} & \text{if } x = \dfrac{p}{2^k} \text{ with } p \text{ odd} \\ 0 & \text{otherwise} \end{cases}$$

The ruler sequence after the linear transformation matches the sequence of exponents of the image of the set of binomial rationals by h, ordered from smallest to largest. For example, restricting the binary rationale to those with powers of n less than 4, the ordered image of h is

$$\frac{1}{2^4}, \frac{1}{2^3}, \frac{1}{2^4}, \frac{1}{2^2}, \frac{1}{2^4}, \frac{1}{2^3}, \frac{1}{2^4}, \frac{1}{2}, \frac{1}{2^4}, \frac{1}{2^3}, \frac{1}{2^4}, \frac{1}{2^2}, \frac{1}{2^4}, \frac{1}{2^3}, \frac{1}{2^4}$$

whose sequence of exponents is

$$-4, -3, -4, -2, -4, -3, -4, -1, -4, -3, -4, -2, -4, -3, -4$$

By adding the highest absolute number plus 1, in this example $4 + 1 = 5$, to each member of the sequence, the series can be changed to produce positive integers:

$$\mathbf{1}, \mathbf{2}, 1, \mathbf{3}, 1, 2, 1, \mathbf{4}, 1, 2, 1, 3, 1, 2, 1, \mathbf{5} \tag{10}$$

Similarly, the infinite ruler series can be obtained by applying the same transformation to any value of n.

3.2 | Ruler transform-based image encryption

Encryption is defined as the process of encoding confidential images using cryptographic techniques so that only authorized users can decipher them.[40] There are three different types of image encryption methods: Substitution, permutation/transposition, and methods that combine both. While permutation schemes merely shuffle the pixel values according to the algorithm, substitution schemes alter the pixel values. In the permutation process, the pixel coordinates of an image are relocated using the matrix transformation.[41] The transformation matrix developed by some integer series mitigates the pixel correlation effectively. The ruler sequence-based transform algorithm preserves uniformity dispersing the neighboring pixels in a manner that they are all equally distant from each other offering the best encryption. A 2×2 matrix formed by four consecutive digits of the ruler sequence is totally unimodular effectively relocating the pixels of a matrix and consequently can be employed for pixel scrambling via encryption. The general equation of ruler transform is a chaotic mapping and is represented as

$$\begin{bmatrix} p(i+1) \\ q(i+1) \end{bmatrix} = \begin{bmatrix} R_i & R_{i+1} \\ R_{i+2} & R_{i+3} \end{bmatrix} \begin{bmatrix} p(i) \\ q(i) \end{bmatrix} \bmod N \tag{11}$$

In Equation (11), p and $q \in \{0, 1, 2, 3, ..., N-1\}$, $\{p(i), q(i)\}$ and $\{p(i+1), q(i+1)\}$ are the old and new coordinates, respectively, R_i is i^{th} term in the ruler series, 'mod' and "N" are the mod operator and size of digital image. By employing ruler transformation, the original pixels of the matrix are replaced by the new ones. Further, denoting $\begin{bmatrix} R_i & R_{i+1} \\ R_{i+2} & R_{i+3} \end{bmatrix}$ as RT_i, the subsequent transformation matrices of the ruler sequence can be formed as follows:

$$RT_1 = \begin{bmatrix} R_1 & R_2 \\ R_3 & R_4 \end{bmatrix} = \begin{bmatrix} 1 & 2 \\ 1 & 3 \end{bmatrix}, RT_2 = \begin{bmatrix} R_2 & R_3 \\ R_4 & R_5 \end{bmatrix} = \begin{bmatrix} 2 & 1 \\ 3 & 1 \end{bmatrix}, \text{so on}$$

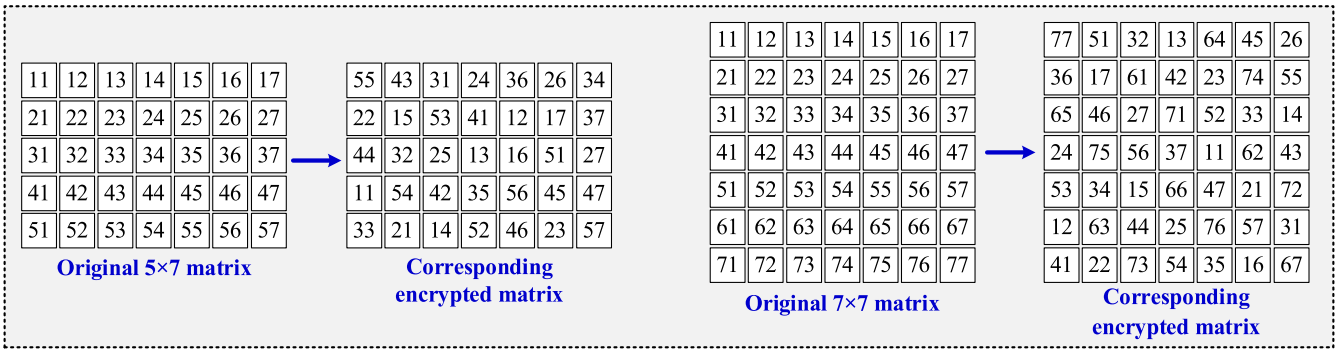

FIGURE 3 Original and corresponding encrypted matrices obtained by the proposed strategy.

The transformation matrices of ruler series can also take on numerous other forms for various i values. Additionally, the scrambling effect is increased by iterating Equation (11) with subsequent operation.

$$\begin{bmatrix} p(i+1) \\ q(i+1) \end{bmatrix} = \begin{bmatrix} R_i & R_{i+1} \\ R_{i+2} & R_{i+3} \end{bmatrix}^n \begin{bmatrix} p(i) \\ q(i) \end{bmatrix} \bmod N, 0n \geq 2 \tag{12}$$

The original and corresponding encrypted matrices obtained by the proposed strategy is shown in Figure 3. It is noted from the figure that all the matrix elements are effectively rearranged having least correlation between them. The generalized pseudocode of RT-based encryption is shown in Algorithm 1.

Algorithm 1: Ruler Transform-based scrambling

Procedure 2D map-based RT encryption

Input: Original matrix 'A' of size (rows, columns, 2)
Output: Encrypted matrix 'B'
[rows, columns] ← matrix dimension
while (termination criteria is not met) **do**
Extract largest symmetrical sub-matrix from (0, 0) coordinates
for i → 1 to rows **do**
    for j → 1 to columns **do**
        s = [i ;j] // obtain old coordinates
        g = mod ((RT*s), dimension) // calculate new coordinates
        new pixel coordinates B(i,j) ← old coordinates A(i,j) // swapping
    end for
end for
Apply the process to all symmetrical sub-matrices
end while

end procedure

3.3 | Application of RT-based encryption in reconfiguration

The predetermined optimal configuration of the solar PV array is obtained using the RT strategy without altering the electrical circuit/connections. Employing this decreases the effects of shading while retaining the electrical characteristics of the PV array. The PV panels configured in a total-cross-tied (TCT) arrangement are physically displaced based on the obtained encrypted RT-matrix pattern. The distinction between the topological architectures of the conventional TCT and the proposed RT is illustrated in Figure 4. For instance, the PV panel designated "25" is located originally in the second row and fifth column (i.e., between Node-B & Node-C) in the TCT configuration of the array. After reconfiguration, this panel is placed in the third row and third column, that is, between Node-C and Node-D based on the resultant encrypted RT matrix (shown in Figure 3), as illustrated in Figure 4. Besides, employing the developed RT matrix, all the PV panels are appropriately reconfigured to disseminate the shadow evenly over the complete array. For example, let us consider that the five panels (designated as PV55, PV43, PV31, and PV24) of the first row of the reconfigured PV array experience shadowing. Due to reconfiguration, this row-wise

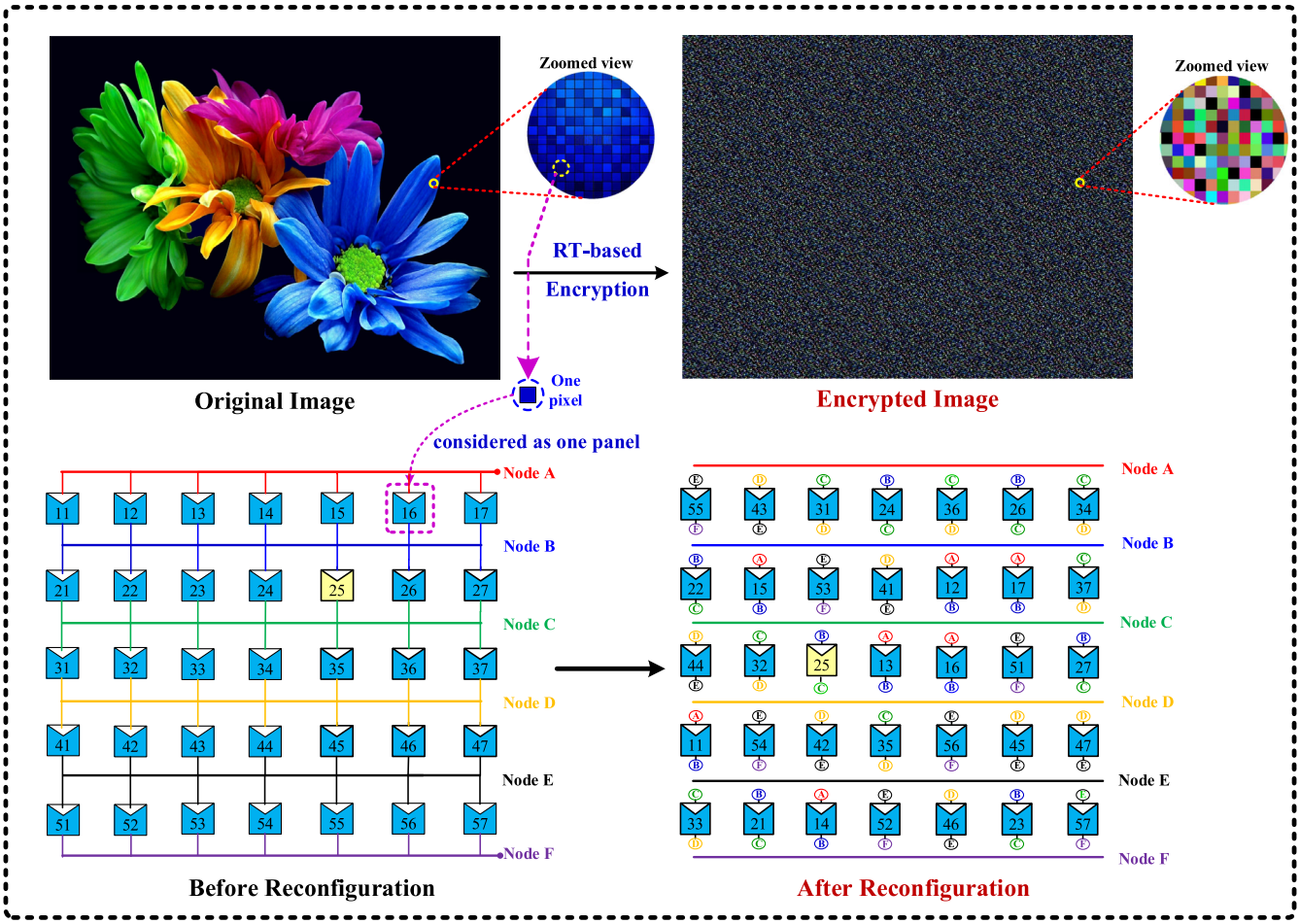

FIGURE 4 Topology reconfiguration based on encryption approach.

shade is dispersed uniformly to all the rows balancing the irradiance levels between the rows. This is because these PV panels are placed physically in the first row however are connected electrically to different rows of the array. Consequently, the suggested ruler transform-based PV array reconfiguration strategy mitigates the mismatch effectively between rows under PS conditions.

3.4 | Radial basis function neural network-based MPPT

The proposed RBF neural network technique[42] predicts the near-optimal duty ratio bringing the operating point of the PV array close to MPP. The obtained near optimal duty ratio is then fed to the conventional INC algorithm as its initial duty ratio. Further, the INC algorithm fine-tunes the estimated duty ratio to bring it to the GMP. This relieves the INC from the problem of being stuck at the local maxima caused due to rapid climatic variations where the duty ratio corresponding to GMP is rightly estimated by the RBF neural network NN (RBF NN) technique. The finally obtained optimal duty ratio is given to the PWM generator, which produces the gating pulses to the boost converter to deliver maximum power from the PV generator for a specified load.

3.4.1 | Radial basis function neural network

In recent days, intelligence-based ANN algorithms are becoming more and more prevalent for solving the most complex problems in various fields of engineering. These algorithms are quite flexible in solving any kind of problem as they don't require any detailed information regarding the system and its mathematical modeling. They function based

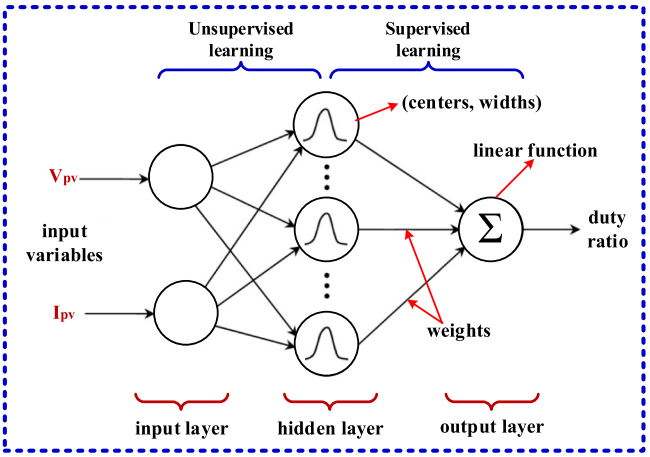

FIGURE 5 Radial basis function neural network.

on the input–output relations. RBF NN is an advanced tool employed in ANNs for classification and predictions based on its training pattern.[42]

It is used commonly for curve-fitting tasks in multidimensional search space. It has an advantage over the widely applied multilayer perceptron (MLP) network model that is designed as a unified computing nonlinear function of the scalar product of the input and weight vectors. When compared to the popular MLP network model, it is advantageous because it is built as a unified computational nonlinear function of the scalar product of the inputs and weights. Because of this advantage, the designed model becomes a multidimensional search space problem for the surface that offers the best fit to the training data.

The RBF NN consists of three layers: (a) Input layer, (b) hidden layer consisting of the Gaussian activation function, and (c) output layer consisting of the linear activation function[43] as shown in Figure 5. The hidden layer is the most important of the three. The training of RBF NN consists of unsupervised and supervised learning. The unsupervised learning is performed between the input layer (i) and the hidden layer (j). In this, center (or mean, μ) and width parameter (or standard deviation, σ) for the Gaussian activation function at each hidden neuron must be computed. The computation of these RBF centers is executed by using the K-means clustering algorithm. The center of each cluster at the hidden layer is then initialized to different randomly selected training patterns (inputs). Further, each training pattern is assigned to the nearest cluster at the hidden layer. This can be accomplished by calculating the Euclidean distances between the training patterns and the cluster centers.[44]

$$\text{Euclidean distance}, E_D(x,c) = \sqrt{\sum_{i=1}^{n} (x_i - c_i)^2} = \sqrt{(x_1 - c_1)^2 + (x_2 - c_2)^2 + (x_2 - c_2)^2 + \ldots + (x_i - c_i)^2}$$

where x_i = training input patterns (x_1, x_2, x_3, x_4, ..., x_n) and c_i = cluster centers (c_1, c_2, c_3, c_4, ..., c_n)

When all the training patterns are assigned, the average position for each cluster center is to be calculated. The calculated average then becomes the new cluster centers (μ). The above procedure is then repeated until the cluster centers remain unchanged for the subsequent iterations. Thus, the center (mean, μ) is calculated at each neuron of the hidden layer. Later, the width parameter (σ_m) of each neuron of the hidden layer[44] is computed using the following equation

$$\sigma_m = \frac{1}{P} \sqrt{\sum_{m=1}^{P} |\mu_{m+1} - \mu_m|^2}$$

where μ_{m+1} are the mean of node $m+1$ and μ_m are the mean of node m. Thereafter, the computed mean (μ) and standards deviation (σ) are substituted in the Gaussian activation function in order to obtain the output (o_j) of each neuron at the hidden layer.

$$\text{Output of Gaussian activation function, } o_j = \frac{1}{\sigma\sqrt{2\pi}} \exp\left[\frac{-(x-\mu)^2}{2\sigma^2}\right]$$

where $x =$ input training patterns, $\mu =$ mean, and $\sigma =$ standard deviation.

Following the execution of unsupervised learning, supervised learning is then performed between the hidden layer (j) and output layer (k). In supervised learning, the weight matrix between the hidden layer and the output layer has to be trained. In this process, the net value of the output layer is calculated and is used for computing the output of the output layer by substituting it in the linear activation function.[44]

$$net_k = \sum_{k=1}^{n}\sum_{j=1}^{n}(w_{jk} * o_j) = w_{11}o_1 + w_{21}o_2 + w_{31}o_3 + \ldots\ldots\ldots\ldots w_{n1}o_n$$

In the output layer (k), the activation function used is linear activation function. Hence, the net value (net_k) is equal to the output value (o_k),

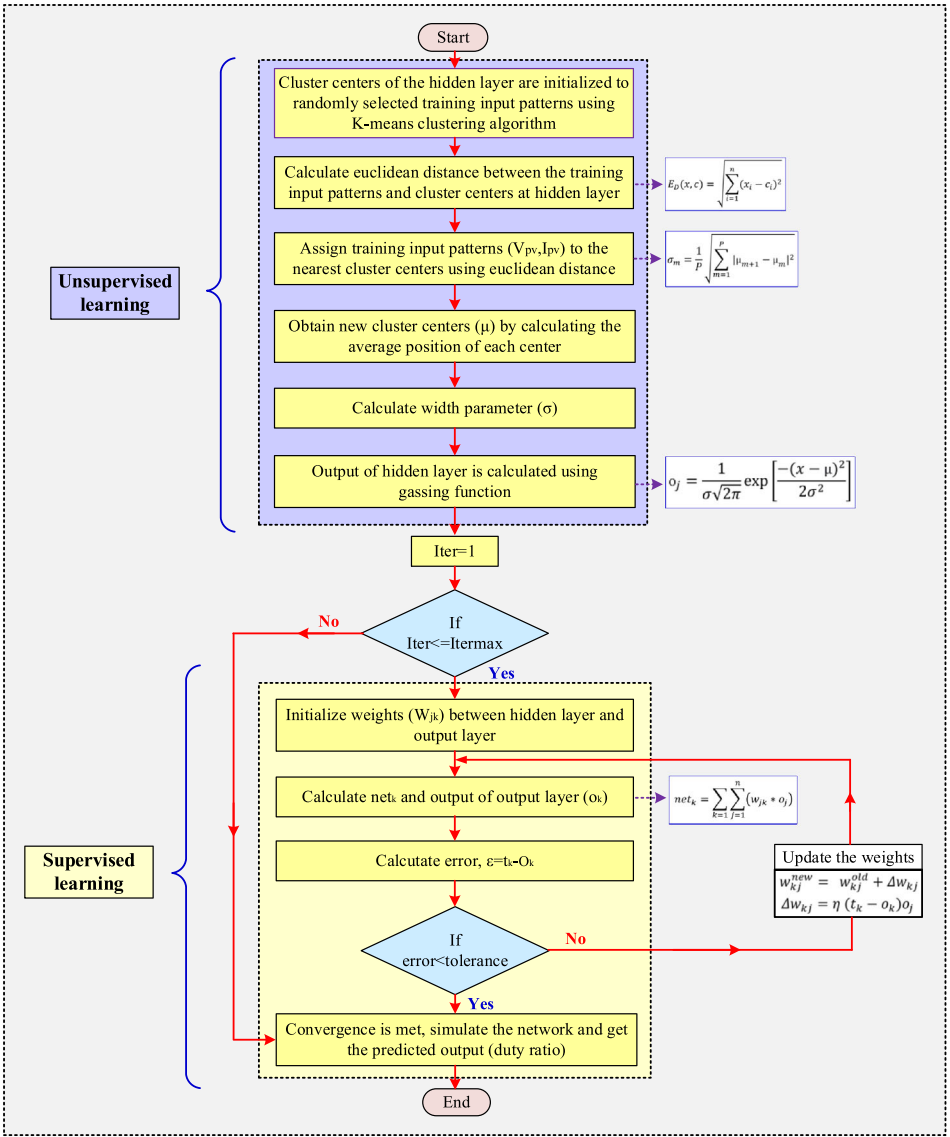

FIGURE 6 Flowchart of the proposed radial basis function neural network.

$$o_k = net_k$$

After computing the output of the output layer, the error between the target output and the calculated output is to be determined as follows

$$\text{error}, \varepsilon = t_k - o_k$$

where t_k = target output and o_k = calculated output.

If the obtained error is not within the tolerance limits, the change in weights is calculated and the weights are updated to new values.

$$\text{Change in weights}, \Delta w_{kj} = \eta\,(t_k - o_k)o_j$$

where η = learning rate, ranging from 0 to 1.

$$\text{new weights}, \; w_{kj}^{\text{new}} = w_{kj}^{\text{old}} + \Delta w_{kj}$$

The process is continued until the error reduces within the tolerance limits. The flowchart of the proposed RBF neural network is shown in Figure 6.

3.4.2 | RBF neural network

In order to obtain the training and testing data sets, a MATLAB Simulink model of the PV system without an MPPT controller is developed. The model is tested under numerous uniform and nonuniform shading conditions and the optimal values of duty ratio for the corresponding shading cases have been recorded accurately. The collected data is then utilized for the training and testing of the RBF model. After collecting the data, the RBF NN is generated (as shown in Figure 7A,B) by using the following command:

net = newrb (in, out, goal, spread, MN, DF) where the terms are expanded as follows:

net: created RBF NN
in: input data
out: target data
goal: mean squared error goal
spread: spread of radial basis function
MN: maximum number of neurons
DF: number of neurons to add between displays

The RBF NN is generated and trained using the training data till the error is reduced to the tolerance limit (1e−32). The performance plot of generated RBF NN is shown in Figure 8. It is noted from the figure that the training error is reduced to 6.92256e−32. Now, the neural network is tested with the testing data and the error is found to be very less. The generated RBF NN is exported to MATLAB Simulink as a block using the gensim command as shown in Figure 9.

4 | RESULTS AND DISCUSSION

To substantiate the performance of the proposed methodology shown in Figure 10, it is tested and analyzed numerically in a MATLAB environment (R2021a, 64-bit version, solver options: variable-step type, the solver is ode23tb stiff/TR-BDF2 and relative tolerance is 1×10^{-6}) with a resistive load of 12.85 Ω. The TCT-configured 5×7 PV array is constructed with 35 Kyocera KC200GT PV panels. The parameters of the overall PV system are grouped in Table A1 of

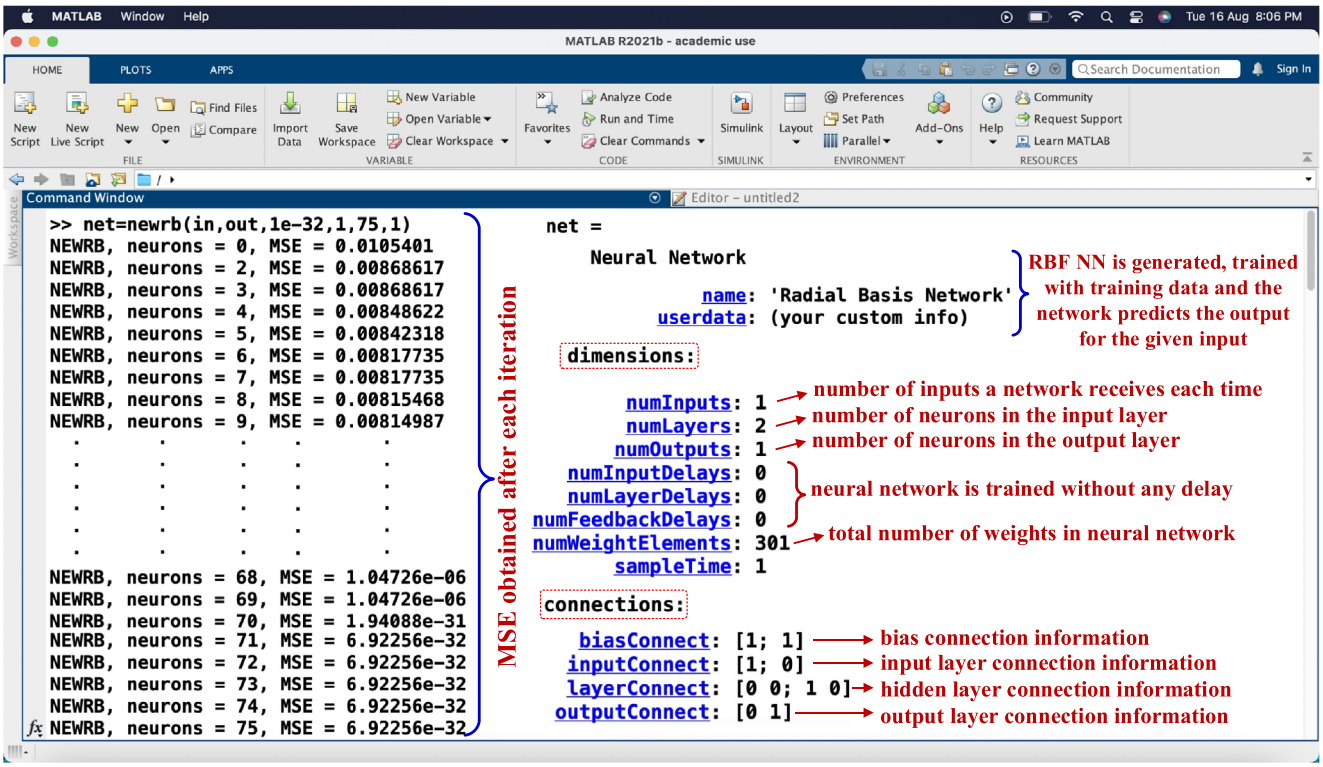

(A)

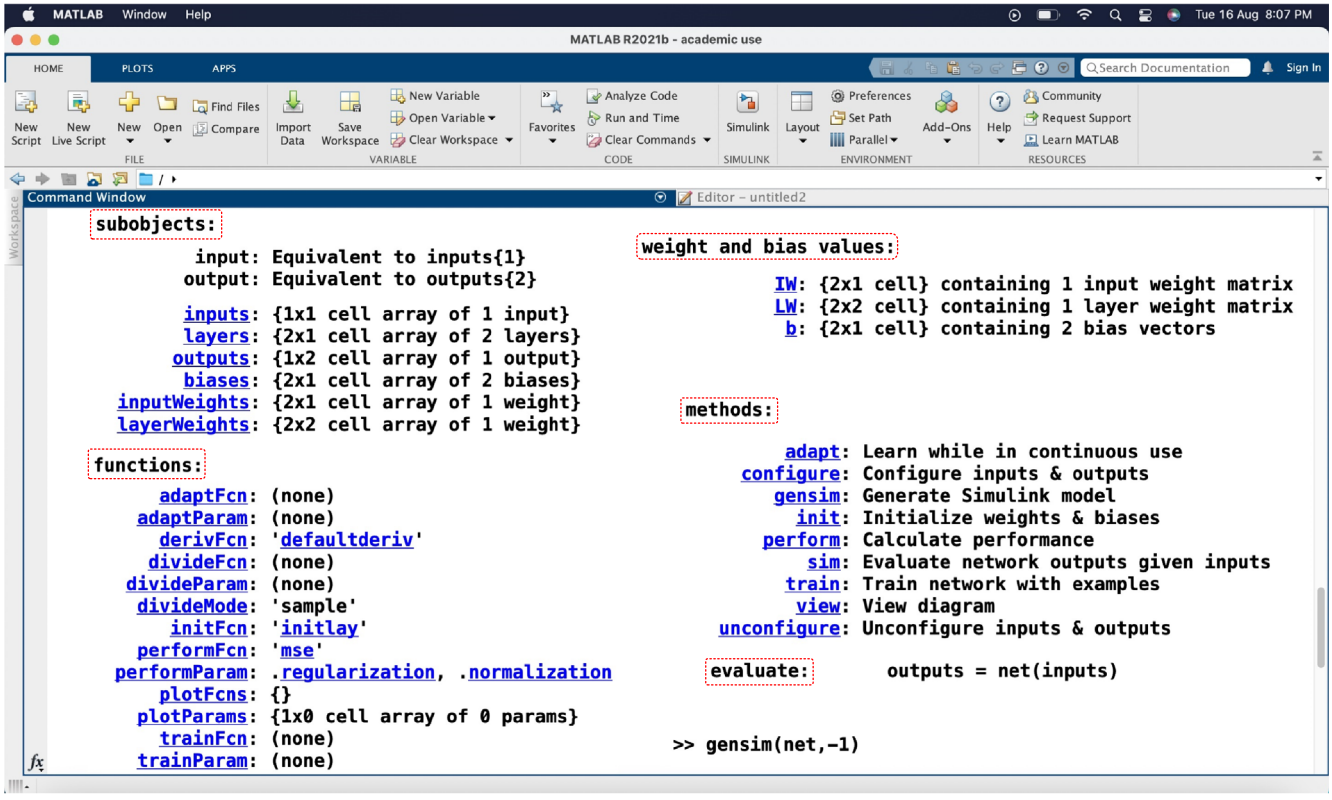

(B)

FIGURE 7 (A,B) Code generated by RBF nntool in MATLAB.

Appendix A. The performance of the proposed RBF and conventional INC-based MPPT techniques has been investigated under various environmental conditions such as uniform, nonuniform, and partial shading conditions. Besides,

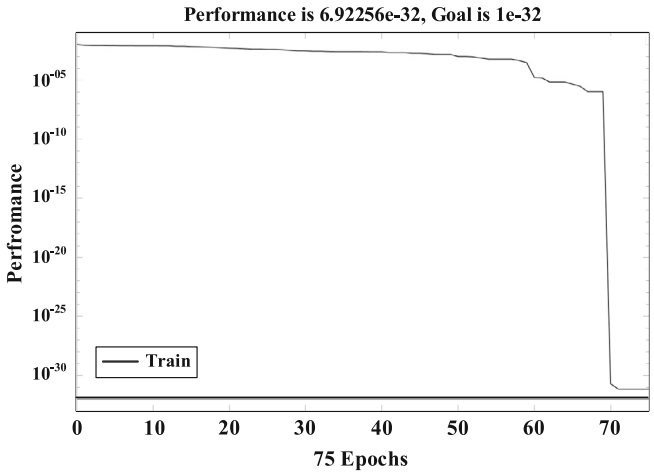

FIGURE 8 Performance plot of generated RBF NN.

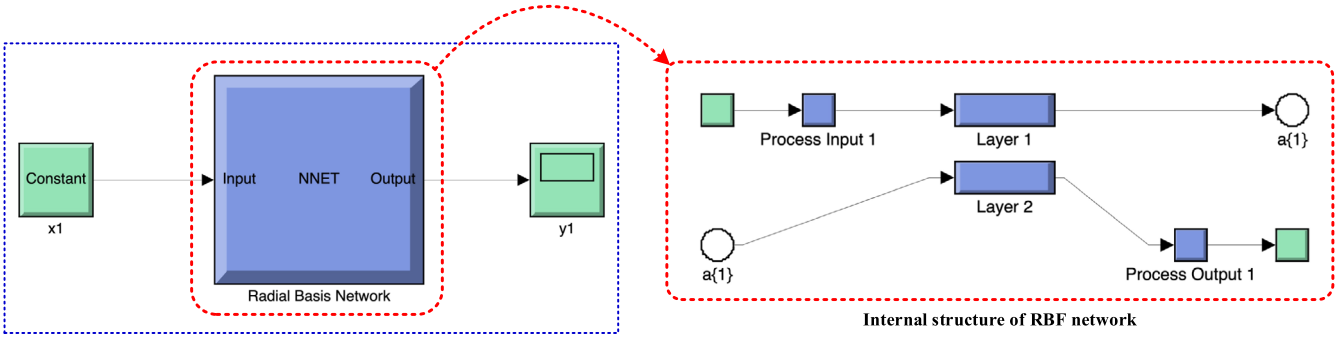

FIGURE 9 RBF network developed using gensim in MATLAB.

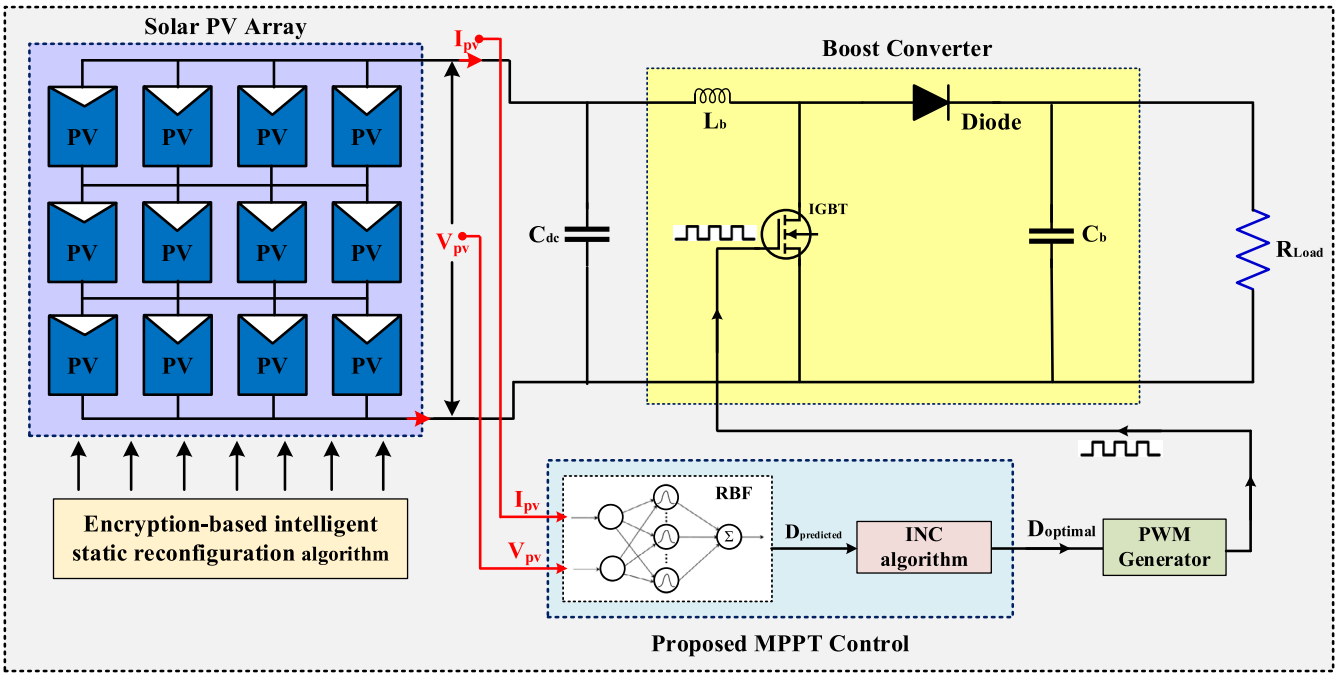

FIGURE 10 RBF NN-based MPPT control of solar PV system.

TABLE 1 Performance indices comparison of conventional INC and proposed RBF under Case-1 to Case-6.

Shading case	Conventional INC						RBF neural network					
	Before reconfiguration			After reconfiguration			Before reconfiguration			After reconfiguration		
	GMP_{act} (W)	$P_{obtained}$ (W)	$P_{mislead}$ (%)	GMP_{act} (W)	$P_{obtained}$ (W)	$P_{mislead}$ (%)	GMP_{act} (W)	$P_{obtained}$ (W)	$P_{mislead}$ (%)	GMP_{act} (W)	$P_{obtained}$ (W)	$P_{mislead}$ (%)
Case-1	4955.0	4127.0	**16.72**	6018.3	6018.3	0	4955.0	4955.0	0	6018.3	6018.3	0
Case-2	4443.3	4128.0	**7.091**	5814.5	5814.5	0	4443.3	4443.3	0	5814.5	5814.5	0
Case-3	5493.0	4613.0	**16.03**	5980.1	5980.1	0	5493.1	5493.1	0	5980.5	5980.5	0
Case-4	5107.0	4453.0	**12.81**	5805.7	5805.7	0	5107.0	5107.0	0	5805.7	5805.7	0
Case-5	4328.4	3803.4	**12.13**	5667.3	5687.3	0	4328.4	4328.4	0	5687.5	5687.5	0
Case-6	3945.1	3784.0	**4.26**	5418.5	5418.5	0	3945.1	3945.1	0	5418.5	5418.5	0

Notes: GMP_{act} = actual GMP; $P_{obtained}$ = obtained ouput; $P_{mislead}$ = misleading power. Bold values indicate the misleading power due to multiple power peaks, which is a significant factor.

TABLE 2 Oscillations around GMP by INC and RBF with and without reconfiguration.

	Range of tracking oscillations in power output							
	Conventional INC				RBF neural network			
Shading case	Before reconfig.	% O_{sc}	After reconfig.	% O_{sc}	Before reconfig.	% O_{sc}	After reconfig.	% O_{sc}
Case-1	~60 W	1.46%	60 W	0.99%	16 W	0.32%	9 W	0.14%
Case-2	280 W	6.79%	83 W	1.42%	21 W	0.47%	10 W	0.17%
Case-3	220 W	4.77%	90 W	1.50%	36 W	0.65%	8 W	0.13%
Case-4	276 W	6.19%	31 W	0.53%	23 W	0.45%	9 W	0.15%
Case-5	227 W	5.97%	63 W	1.11%	24 W	0.55%	12 W	0.21%
Case-6	403 W	10.65%	41 W	0.76%	42 W	1.64%	22 W	0.40%

Note: % O_{sc} = percentage tracking oscillations in output.

the Ropp test and sine radiation test have been employed to validate the proposed approach. The present analysis majorly focuses the radiation effect alone because the radiation impact on the PV system is dominating in relation to ambient temperature. The day-to-day sun's radiation typically has abrupt fluctuations. The comparison of performance indices, oscillations around GMP obtained by the conventional INC and proposed RBF under Case-1 to Case-6, is given in Tables 1 and 2, respectively. The performance analysis is carried out as follows.

4.1 | Analysis under uniform shading conditions

During the uniform shading conditions, all the panels of an array are uniformly shaded receiving lower irradiation levels. The Ropp irradiation and sine irradiation profiles are popularly used to validate the effectiveness of the MPPT controller in the tracking of GMP for gradual and impulse step variations in radiation. Further, it also comprises steady-state conditions. The Ropp irradiation profile is significantly dynamic containing distinct gradual (linear rising/falling slopes) and sudden/step variations, whereas the sine irradiation profile contains only gradual variations as shown in Figure 11A,B. The sine profile is close to reality where the irradiation change couldn't be dynamic and may vary gradually/nonlinearly unlike the Ropp profile. Both tests are conducted to examine the tracking of the MPPT controller during sudden and changing irradiation rates at all sampling times. The output power obtained by the proposed RBF approach for the corresponding Ropp and sine irradiation profiles is shown in Figure 11C,D. It is remarked from the figure that the RBF-based algorithm tracks the GMP within 0.04 s for a step change in irradiation (from the zoomed view of Figure 11C), and it tracks the gradual changes following the sine irradiation pattern accurately without any delay (from Figure 11D). The obtained steady-state oscillations for the sine profile are less than 4 W as shown in the zoomed portion of Figure 11D. Hence, it is remarked that the proposed RBF tracks the GMP rapidly with around zero steady-state oscillations under uniform shading conditions.

The RBF neural network controller output curve is shown in Figure A1 of Appendix A. It is noted from the figure that the proposed controller predicts the optimal duty ratio based on the training data and tracks the global power point effectively and rapidly with fewer oscillations.

4.2 | Analysis under partial shading conditions

In practice, the PV arrays are commonly subjected to partial shading (PS) conditions where a part of the array receives lowered irradiation while the remaining part receives maximum irradiation. This is mainly caused due to neighboring buildings, rooftop chimneys, long trees, dust and snow accumulation, bird droppings, and so forth. Hence, it is essential to study the performance of the proposed reconfiguration scheme along with the novel RBF-based MPPT scheme under PS conditions. The proposed scheme has been tested and analyzed for five distinct PS conditions shown in Figure 12.

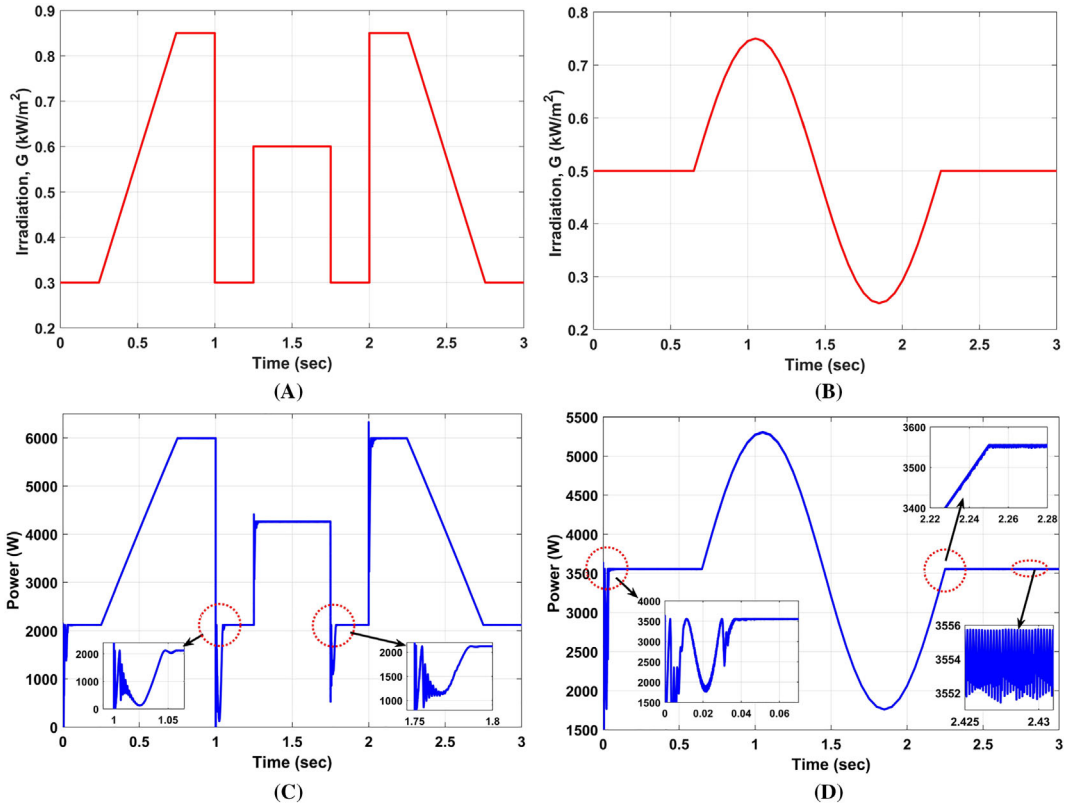

FIGURE 11 Irradiation profiles of (A) Ropp test and (B) sine test, (C,D) corresponding output power obtained.

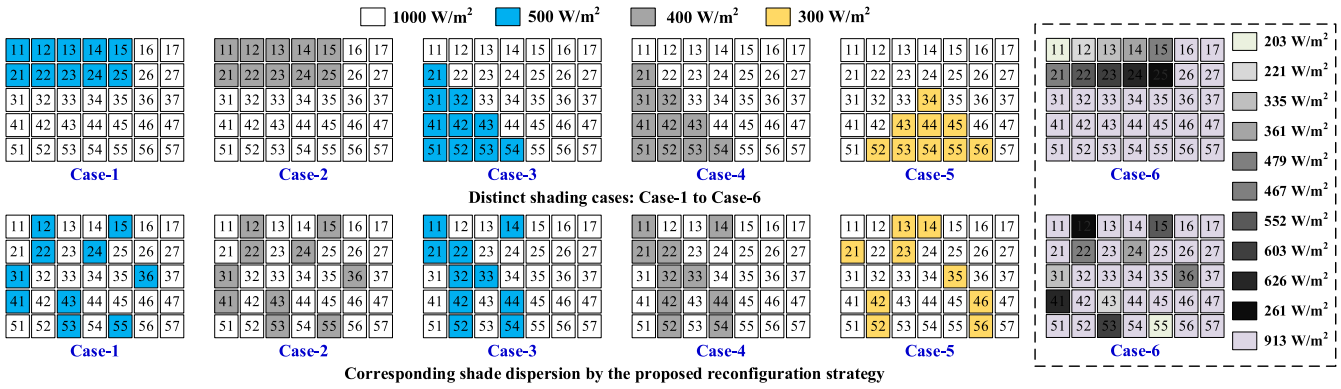

FIGURE 12 Various shading cases and respective shade dispersion obtained by RT-based encryption strategy.

4.2.1 | During Case-1 shading condition

In this case, the PV array experiences a rectangular shading pattern where the unshaded and shaded panels receive 1000 W/m^2 and 500 W/m^2 as shown in Case-1 of Figure 12. Due to this mismatch between the rows of the PV array, the array exhibits an LMPP.

So, the conventional INC algorithm gets stuck at this LMPP and yields a suboptimal output of 4127 W as shown in Figure 13A. The RT-based reconfiguration disperses the shade uniformly minimizing the mismatch to zero thereby augmenting the GMP and eliminating the LMPP. Hence, the array characteristics are improved yielding the enhanced GMP of 6018.3 W. After reconfiguration, the conventional INC is now able to track the GMP of 6018.3 W without being stuck at LMPP (from Figure 13B). On the contrary, before reconfiguration, the proposed RBF doesn't get stuck at LMPP

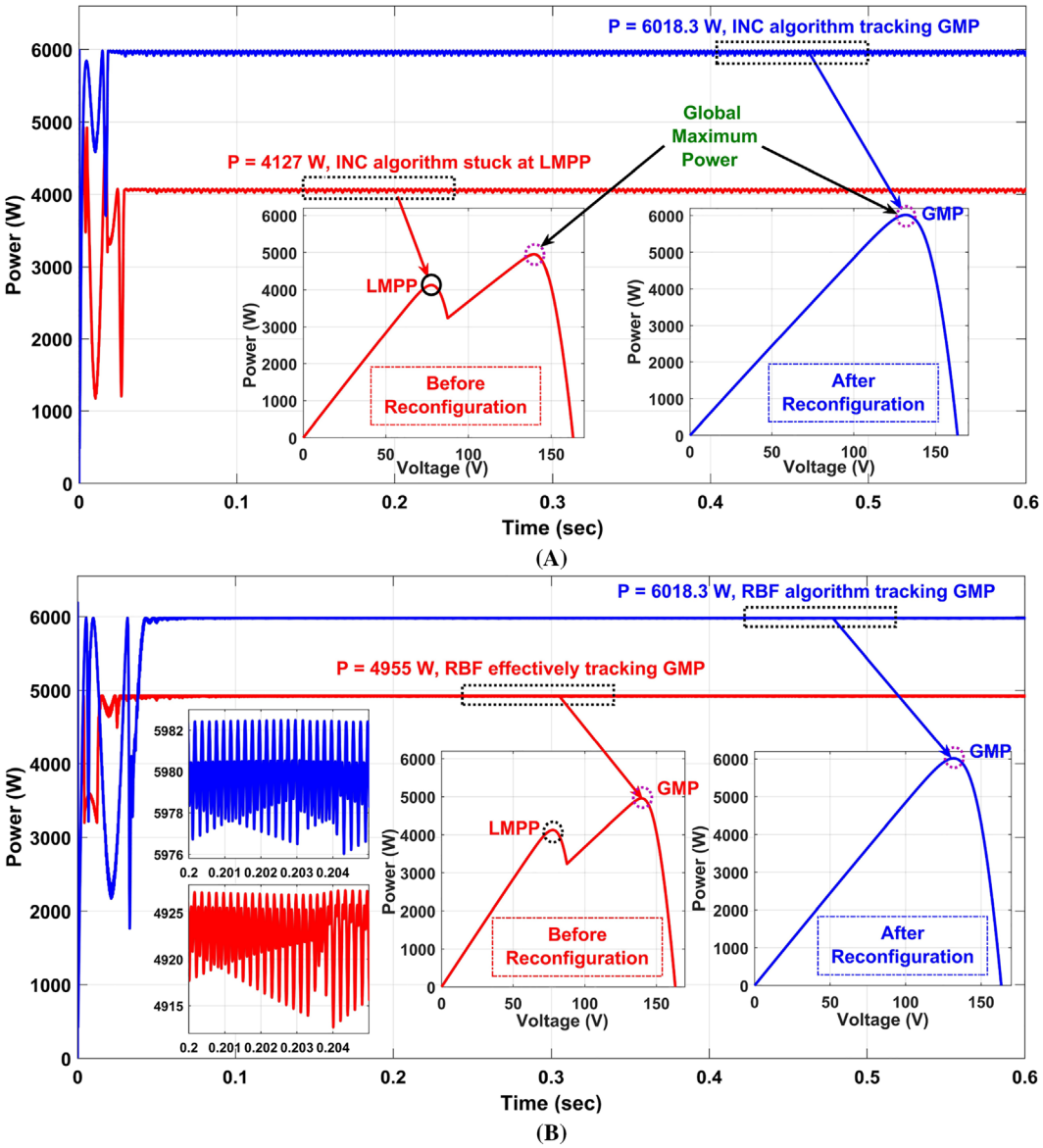

FIGURE 13 PV array power obtained by (A) conventional INC and (B) proposed RBF under Case-1.

(unlike INC) and tracks the GMP of 4955 W, and after reconfiguration, it tracks the improved GMP of 6018.3 W. Even though the conventional INC tracks the GMP effectively after reconfiguration, the output power oscillates within the range of 60 W. Further, these oscillations are reduced to less than 9 W with the proposed RBF scheme for the reconfigured PV array. It is noted from Figure 13 that the tracking speed of the INC algorithm is improved significantly after reconfiguration. The RBF tracks the GMP of 4955 W for the non-reconfigured array, which is 21.46% less than that of the reconfigured array.

4.2.2 | During Case-2 shading condition

In Case-2, the similar shading pattern studied in Case-1 is considered by slightly lowering the shaded panel irradiation to 400 W/m^2. When compared to the previous case, the reduction of irradiation levels by 100 W/m^2 in the present case causes significant oscillations by the conventional INC, which is up to 280 W (Figure 14A), whereas the oscillations in Case-1 are up to 60 W. After reconfiguration, both the INC and proposed RBF successfully tracked the GMP of

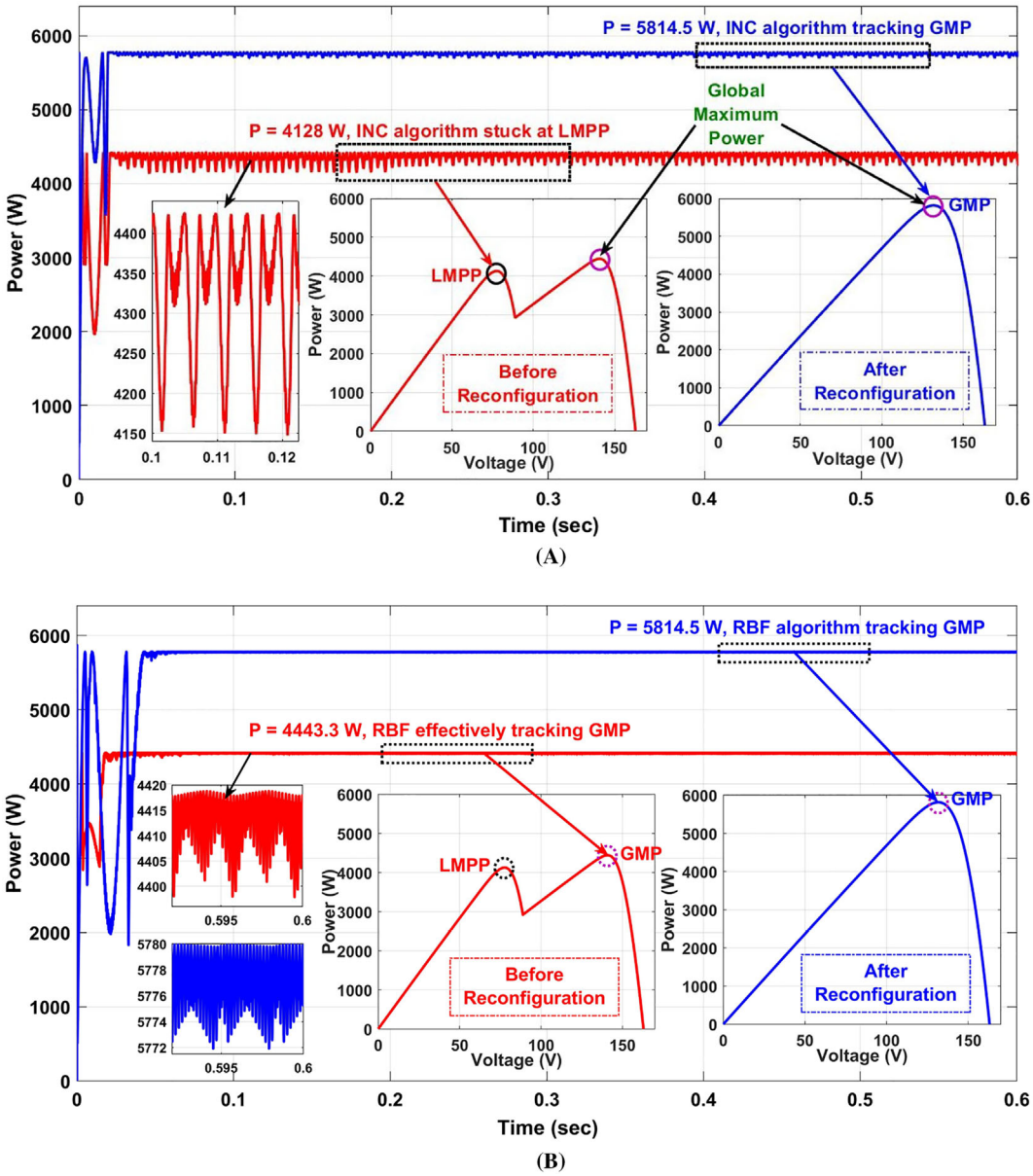

FIGURE 14 PV array power obtained by (A) conventional INC and (B) proposed RBF under Case-2.

5814.5 W due to the elimination of the LMPP. It is noted in Figure 14A,B that after reconfiguration, the GMP tracked by both INC and RBF approaches is enhanced by 40.86%.

4.2.3 | During Case-3 shading condition

A triangular shading pattern with shaded panels receiving 500 W/m^2 is considered in Case-3 of Figure 12. Before reconfiguration, the PV array exhibits four LMPPs and one GMPP at 5493 W. Due to the numerous LMPPs, the INC algorithm is stuck at one of the LMPPs and yields a lowered output of only 4613 W. However, after reconfiguration, the concentrated shading has been effectively dispersed thereby equalizing the irradiations in all rows of the PV array. This eliminates all the LMPPs and exhibits a single power peak in the array characteristics. Hence, the conventional INC easily tracks the GMP (of 5980.5 W) as the problem of being stuck in the LMPP is evaded. Additionally, for the reconfigured array, the oscillations in tracking are also greatly reduced compared to that of the non-reconfigured array.

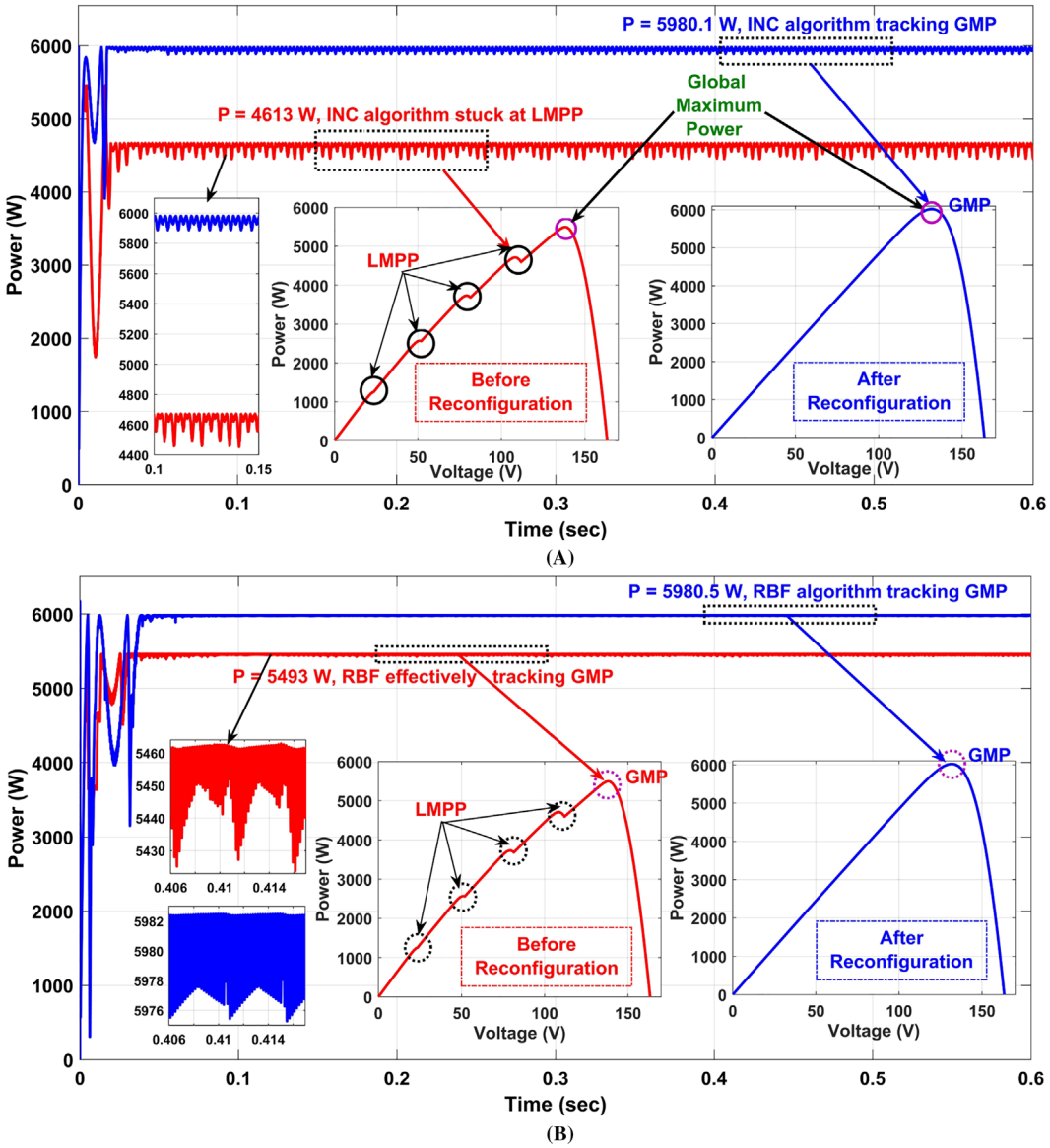

FIGURE 15 PV array power obtained by (A) conventional INC and (B) proposed RBF under Case-3.

Unlike INC, the proposed RBF doesn't get stuck at LMPP and employing it yields the GMP of 5980.5 and 5493 W for the reconfigured and non-reconfigured arrays, respectively (Figure 15B). The steady-state oscillation of the proposed RBF and INC approaches after reconfiguration is also predominantly reduced as shown in Figure 15A,B.

4.2.4 | During Case-4 shading condition

During Case-4, the same triangular shading pattern studied in Case-3 has been considered by slightly lessening the shaded panel irradiation to 400 W/m^2 (Figure 12). As noted in the previous case studies, the conventional INC gets stuck in the local power peak operating the PV array at a suboptimal point delivering only 4453 W (Figure 16A). However, the reconfigured PV array yields only a single peak through its intelligent shade dispersion process and tracks the GMP of 5805.7 W, which is 30.38% more compared to the conventional PV array. Similar to the previous case studies, the RBF doesn't get stuck at LMPP. Further, the steady-state oscillations are also greatly reduced with the RBF before and after reconfiguration (Figure 16B).

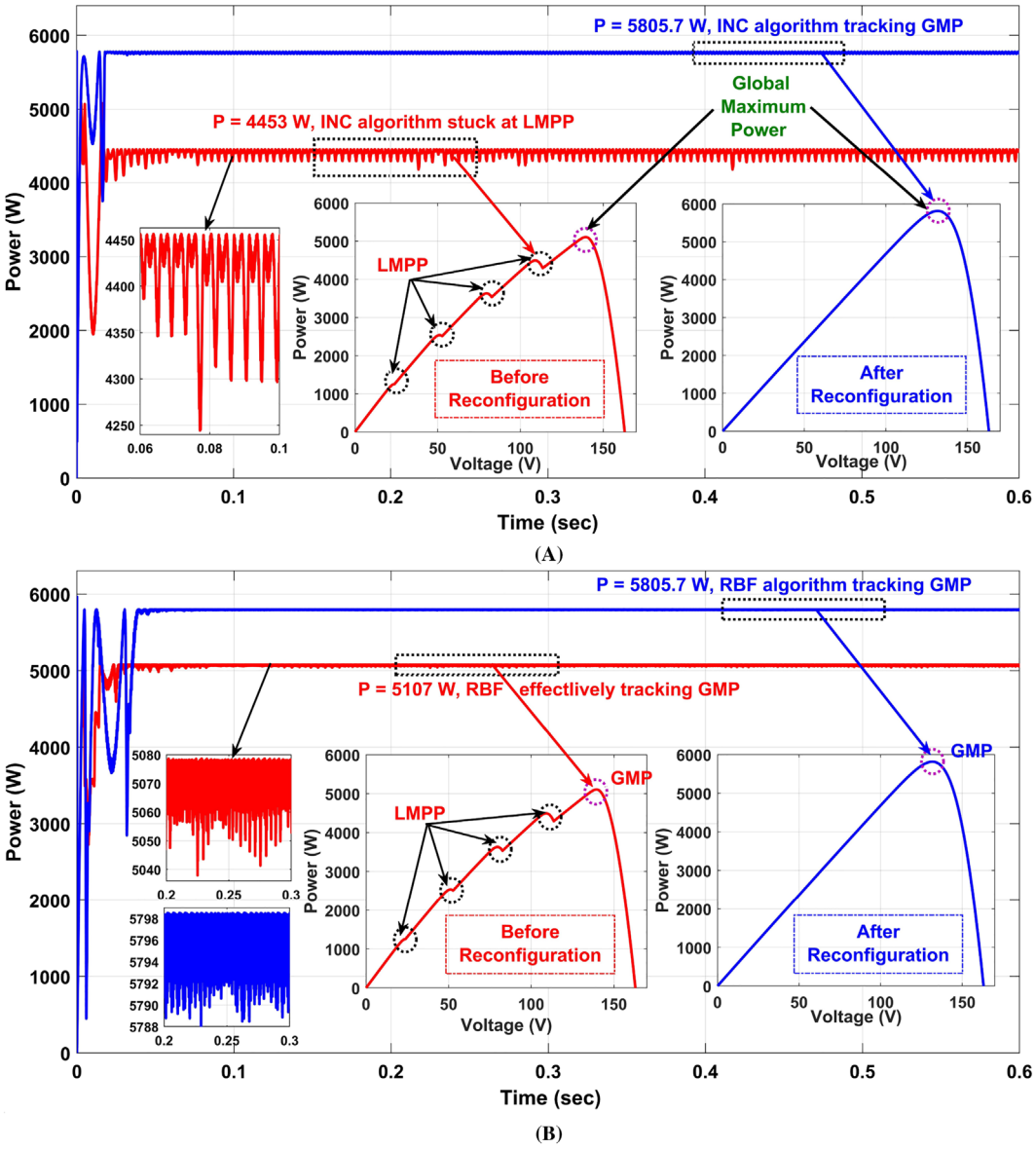

FIGURE 16 PV array power obtained by (A) conventional INC and (B) proposed RBF under Case-4.

4.2.5 | During Case-5 shading condition

Under this case, a complex pyramid patterned partial shading condition is considered for validation where the shaded PV panels receive the irradiation of 300 W/m^2 (Figure 12). The PV array exhibits three LMPPs and one GMP in the array characteristics. Once again, before reconfiguration, the conventional INC algorithm gets stuck at an LMPP tracking a suboptimal output of 3803.4 W (Figure 17A). Besides, the INC algorithm underperforms with a larger settling time (Figure 17A) and yields the GMPP tracking oscillations of about 227 W. These drawbacks are rectified by reconfiguration yielding the improved GMP of 5667.3 W with reduced oscillations. Further, using the RBF approach, the GMP is tracked effectively before and after reconfiguration with comparatively lowered steady-state oscillations as given in Figure 17B.

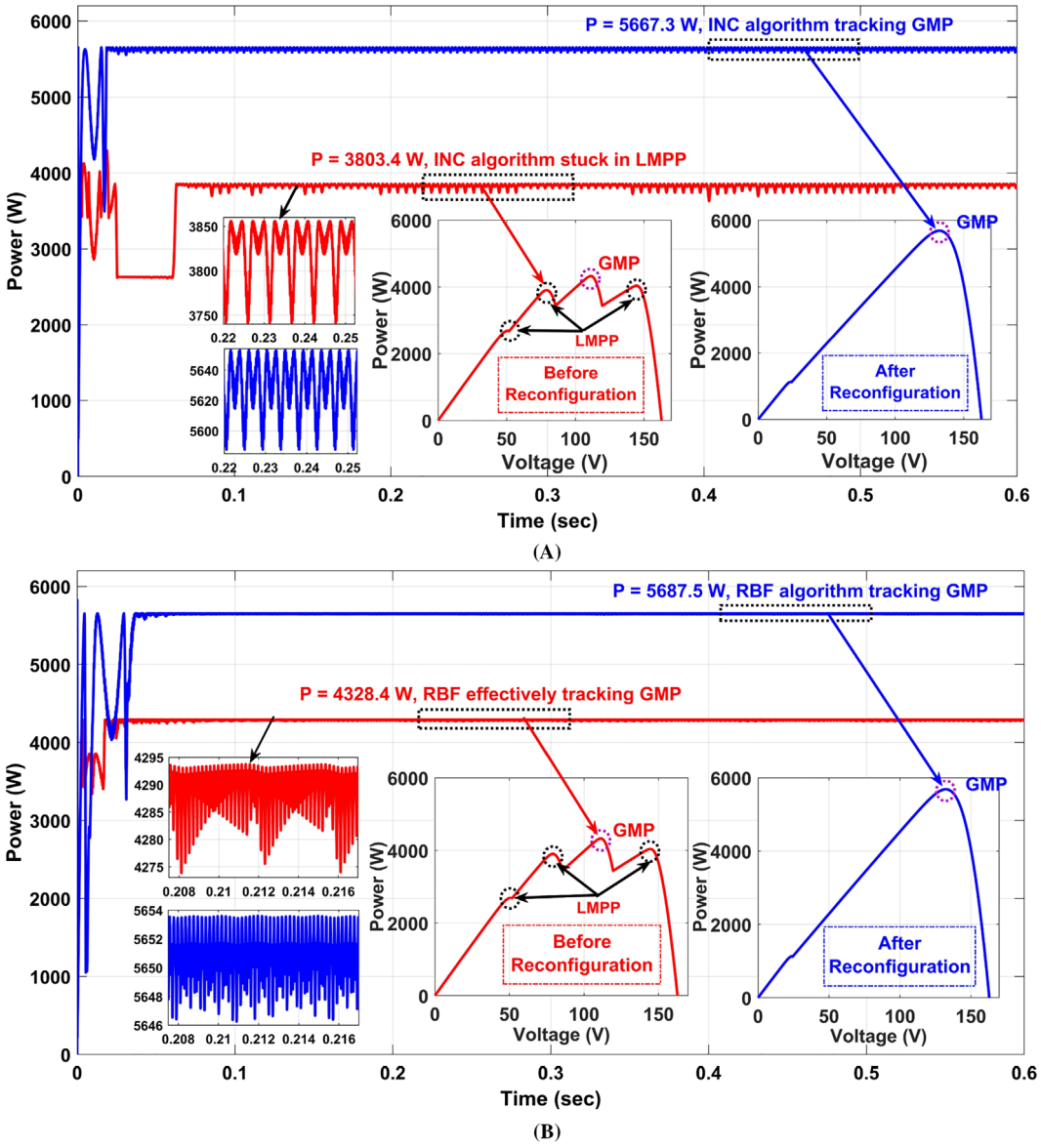

FIGURE 17 PV array power obtained by (A) conventional INC and (B) proposed RBF under Case-5.

4.2.6 | During Case-6 shading condition

During Case-6, a special shading case scenario is considered where the irradiance levels of the adjacent PV panels (of the shaded portion) slightly vary in an increasing or decreasing order as shown in Figure 12. In this case, the unshaded panels are considered to receive the irradiation of 913 W/m^2 and the shaded ones receive the irradiations less than that of 913 W/m^2. The conventional and the proposed methods are tested under this case.

Under this case, the PV array exhibits three power peaks before reconfiguration in which the conventional INC gets stuck in the local optimum yielding the output of 3784 W only (as shown in Figure 18A). However, the proposed RBF tracks the global power peak effectively generating the output of 3945.1 W. Further, upon executing the proposed reconfiguration strategy, the mismatch is significantly mitigated thereby eliminating the two multiple (local power) peaks and enhancing the global power (shown in Figure 18B). Hence, the GMP is enhanced to 5418.5 W and its tracking becomes very easy and accurate without getting stuck in the local optimum. Even the conventional INC algorithm (which is quite simple and cost-effective) is sufficient to track the GMP effectively under shading conditions.

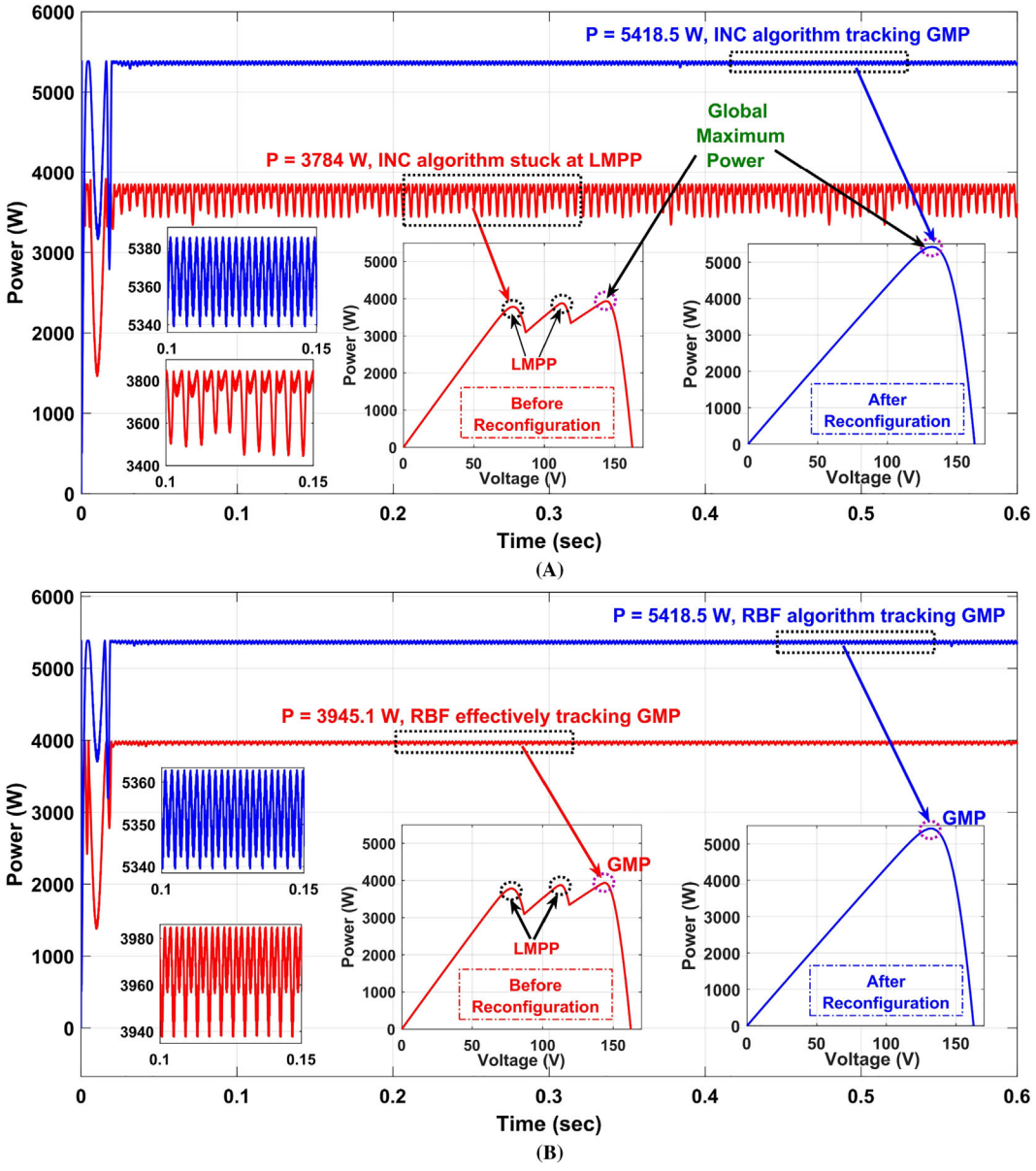

FIGURE 18 PV array power obtained by (A) conventional INC and (B) proposed RBF under Case-6.

For the overall analysis, it is remarked that before reconfiguration, there exist numerous LMPPs in the array of characteristics and hence the conventional INC gets stuck at one of the LMPPs and yields suboptimal output. On contrary, the proposed RBF approach effectively tracks the GMP without being stuck at LMPP. Eventually, it is noteworthy to state that after reconfiguration, the GMP is enhanced significantly due to the considerable mitigation of the mismatch between the rows. Consequently, both the conventional INC and proposed RBF track the GMP effectively with reduced steady-state oscillations. In comparison to the INC, the proposed RBF further yields fewer oscillations as detailed. However, the recently developed advanced and sophisticated MPPT schemes based on neural networks, metaheuristic optimization, fuzzy logic, machine learning, and so forth, despite being efficient theoretically, are hardly employed in the real-time applications of PV systems. In practical scenarios and commercial applications, most of the PV systems are integrated with the conventional MPPT algorithms such as INC and P&O due to their simplicity and cost-effectiveness. Hence, the conventional INC is sufficient to track the GMP of the PV array with reconfiguration but with minimum steady-state oscillations. On the other hand, the proposed RBF can be deployed if the complexity and economy are compromised.

The comparison of proposed RBF and proposed reconfiguration strategy with the state-of-the-art algorithms is shown in Tables 3 and 4, respectively. Figure 19 depicts the GMP enhancement obtained by INC and proposed RBF after reconfiguration.

4.3 | Overall comparison of proposed methodologies with existing ones

This section details the qualitative comparison of the proposed reconfiguration and MPPT strategies with what has been presented in the literature, using specific parameters. The comparison of various reconfiguration strategies with the proposed ones has been given in Table 5.

TABLE 3 Comparison of proposed RBF with the state of art MPPT algorithms.

Parameter	CSA[6]	JAYA[7]	GWO[8]	PSO[6]	LPSO[9]	ACO-NPU[6]	ACO-NPU-PSO[6]	Proposed RBF
Escapes local maxima	Yes	Yes	Yes	Yes	Yes	Yes	Yes	Yes
Tracking speed (s)	0.77	2.85	1.3	2.25	20	2.15	1.3	0.04
Tracking accuracy (oscillations)	Yes (low)	Yes (high)	Yes (high)	Yes (high)	Yes (med)	Yes (high)	Yes (low)	Almost negligible
Tracking efficiency (%)	99.57	99.22	98.9	98.86	97.01	98.67	99.68	99.51
Algorithm complexity	High	High	High	High	High	Very high	Very high	Less
Implementation	Medium	Medium	Complex	Medium	Complex	Complex	Complex	Relatively simple

TABLE 4 Comparison of proposed reconfiguration strategy with the state of art algorithms.

Parameter	EAR-based[23,24]	Optimization-based[19–22]	AI-based[25,26]	Puzzle-based[28]	Chaotic-based[29]	Number-based[32]	Shift-based[33]	Proposed RT
Scalability	High	High	High	Very low	Very low	High	Very Low	High
Shade dispersion	Poor	High	Medium	Medium	Medium	Very poor	Medium	High
Consistency	Medium	High	Medium	Poor	Poor	Very poor	Poor	High
No. of MPPs	High	Low	Medium	Medium	Very high	Very high	High	Low
Need for sensors & switches	Very high	High	High	Nil	Nil	Nil	Nil	Nil

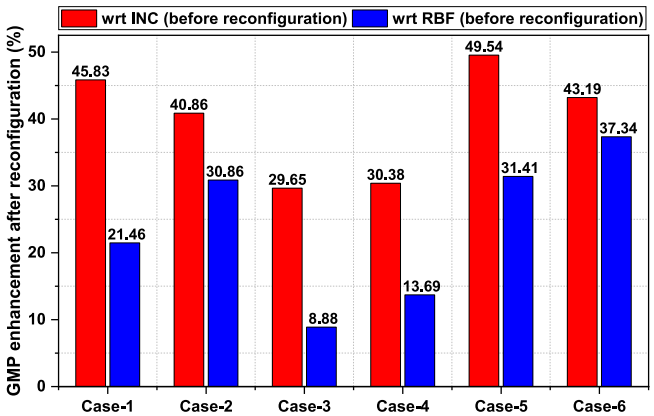

FIGURE 19 GMP enhancement obtained by INC and proposed RBF after reconfiguration.

TABLE 5 Qualitative comparison of various reconfiguration strategies with proposed ones.

Technique	C_1	C_2	C_3	C_4	C_5	C_6	C_7	C_8	C_9
Conventional[18]	VH	L	-	VH	VH	-	-	VL	L
Optimization[19–22]	VH	H	H	L	L	H	VH	VH	VH
Puzzle-pattern[28]	L	M	M	M	M	L	-	L	L
Magic square-based[30]	VL	M	M	M	M	L	-	L	L
Sequence-based[33]	L	M	L	H	M	VL	-	L	L
Analytic-based[32]	VH	M	VL	VH	VH	VL	-	M	L
Chaotic-based[29]	M	M	M	M	H	M	-	M	L
Artificial intelligence[13,14]	H	M	VL	H	H	M	VH	H	VH
Electrical array reconfig[23,24]	M	M	VL	H	H	M	VH	H	VH
Proposed	VH	VH	VH	VL	VL	VH	-	L	L

Note: (C_1) compatibility, (C_2) power yielded, (C_3) shadow dispersion, (C_4) row current difference, (C_5) multiple power peaks, (C_6) constancy, (C_7) switches & sensors, (C_8) algorithm complexity, (C_9) overall cost. (-): nil, V = very, L = low, M = medium, H = high.

4.3.1 | Comparison of proposed reconfiguration approach with state-of-the-art techniques

The effectiveness of the proposed reconfiguration in comparison to current state-of-the-art techniques in terms of several parameters has been listed in Table 4.

- The proposed approach, in contrast to AI approaches[13,14] such as fuzzy logic-based, does not need a switching matrix, or optimal switching matrix selection, and further, avoids memory-related switching matrix operating difficulties.
- The EAR-based solutions[23,24] need a controller to supply the power electronic switches with switching pulses that correspond to the necessary shade dispersion. In addition, a large number of switching patterns are required to determine the best PV array reconfiguration strategy. Contrarily, the proposed method does away with the requirement for them.
- The proposed methods circumvent the shortcomings of population-based meta-heuristic optimization algorithms[19–22] such as wide dimensional search space, convergence issues, parameter choice issues, trapping at local optimum, weighting factor screening difficulties, enormous computations, and increased processing time.
- The proposed approaches, in contrast to the current logic- and puzzle-based methodologies,[28,31] are easily deployable and suitable with all array sizes. Additionally, the presented configuration evenly and discriminately distributes the shadow through the intelligence involved in its encryption-based approach procedure.
- There is a considerable mismatch within PV array when using chaotic techniques[29] because of the extremely strong correlations between the row-wise modules and the diagonally oriented panels. The proposed method, in contrast, greatly reduces the row current mismatch in the array by significantly reducing the correlation between the adjoining panels (in the column, diagonal, and row-wise directions).
- The proposed strategy effectively addresses a number of shortcomings of the previous magic square-based,[30] and sequence-based,[33] approaches, including limited scalability, strong correlations between the diagonal arrangement of modules, and inconsistencies.
- The contemporary OE[32] and OEP[32] approaches provide inconsistent performance with a strong correlation between the subsequent panels row-wise, despite being extensible to any array size. The proposed approach, in contrast, not only has global compatibility but also consistently functions effectively in shaded conditions.

4.3.2 | Comparison of proposed MPPT technique with state-of-the-art techniques

The effectiveness of the proposed MPPT strategy in comparison to current state-of-the-art strategies in terms of various parameters has been listed in Table 4.

- The conventional MPPT algorithms despite being employed widely in the practical applications fail to track the global power peak under shading conditions getting trapped in the local maxima in contrast to the proposed RBF strategy.
- When compared to the existing metaheuristic optimization-based MPPT algorithms,[6–8] the proposed strategy doesn't involve gigantic computation procedures, parameter initialization challenges, computational burden, and convergence issues.

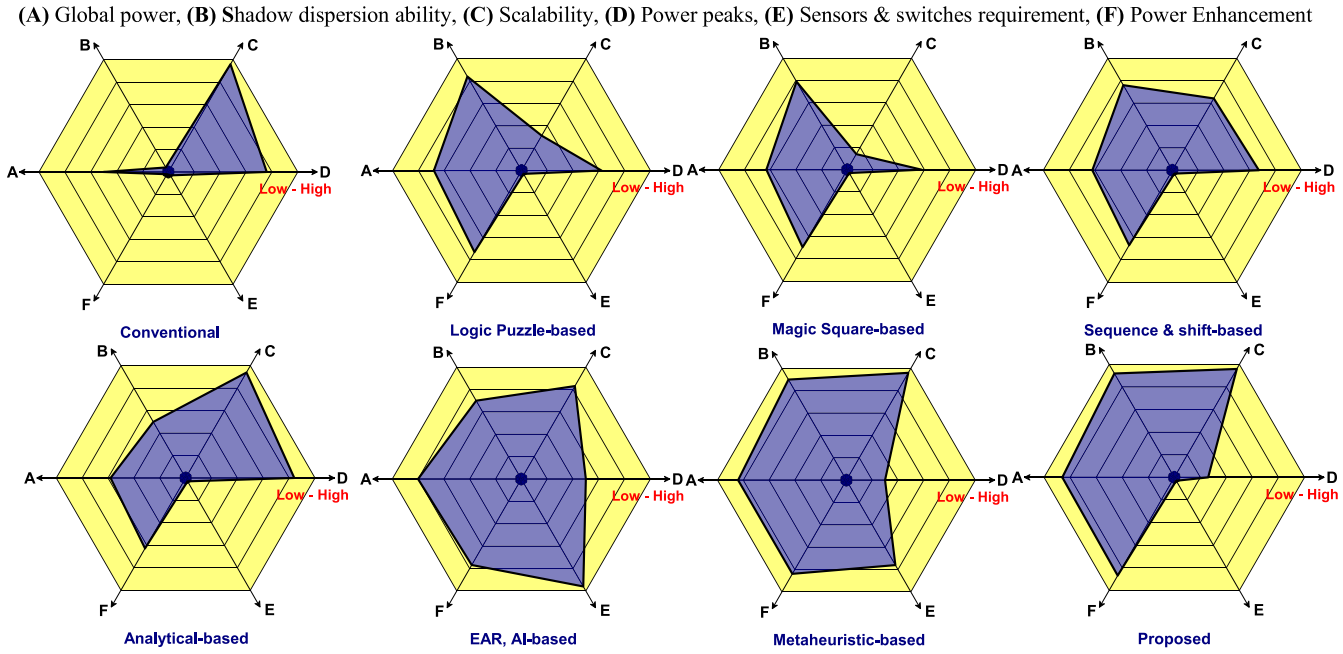

FIGURE 20 Radar charts depicting the comparative performance analysis of various reconfiguration strategies.

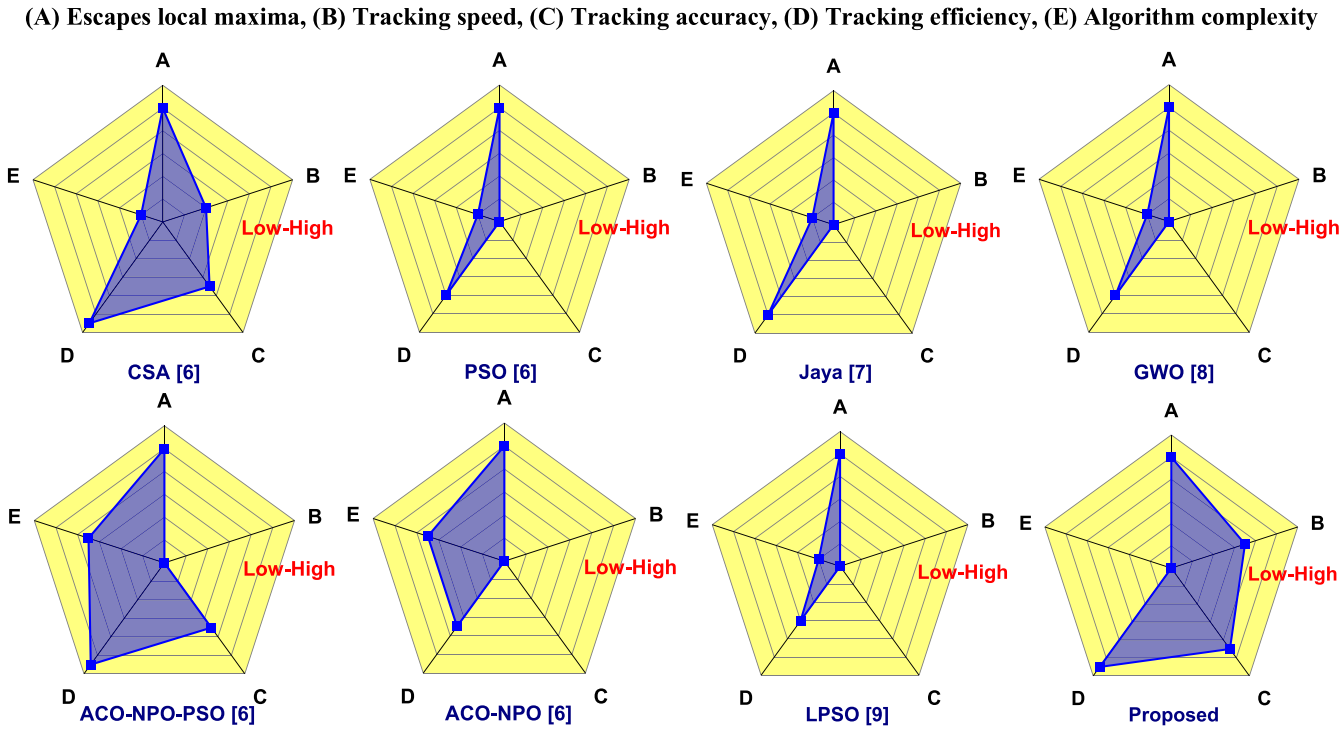

FIGURE 21 Radar charts depicting the comparative performance analysis of various MPPT strategies.

- Further, despite being effective, the hybrid-metaheuristic MPPT algorithms[6] inherit more complexities than the individual algorithm and hence the computational burden is considerably larger than the proposed strategy.
- Unlike the fuzzy logic rule-based computing MPPT techniques[13,14] that necessitates the knowledge of the precise model and the programmer's experience for periodic tuning, the proposed strategy is simple and easy in implementation.

It is clearly evident from the Figures 20 and 21 that the proposed reconfiguration and MPPT strategies exhibit superior performance under shading conditions.

5 | CONCLUSIONS

In this paper, the respective intelligent encryption-based ruler transform (RT) reconfiguration approach and novel RBF NN MPPT-based strategies are proposed to enhance and track the GMP accurately with the least steady-state oscillations. The proposed strategies are validated for a 5 × 7 PV array under various dynamic, uniform and nonuniform shadings. The proposed RBF's results have been contrasted with those of the existing INC algorithm. The major conclusions of the propose work are as follows:

- The INC algorithm gets stuck at local optima yielding poor performance before reconfiguration, but the proposed RBF approach effectively tracks the GMP without being stuck at LMPP.
- After reconfiguration, the GMP is augmented significantly due to the mitigation of mismatch between the rows. Hence, both the conventional INC and proposed RBF effectively track the GMP with fewer steady-state oscillations. However, when compared to INC, the proposed RBF-based MPPT tracks with even lesser oscillations.
- Despite being theoretically effective, the recently developed sophisticated MPPT techniques that incorporate neural networks, metaheuristic optimization, fuzzy logic, machine learning, and so forth are hardly used in real-time PV systems applications due to many limitations, whereas for the proposed reconfigured PV array, a conventional INC algorithm is sufficient to track the GMP but at the cost of a few steady-state oscillations. However, if complexity and economy are compromised, the proposed RBF algorithm can be used for tracking.
- By employing the proposed reconfiguration scheme, the GMP tracking with the conventional INC is improved by 45.83%, 40.86%, 29.65%, 30.38%, 49.54%, and 43.19% for Case-1 to Case-6, and the tracking with the RBF-based MPPT is improved by 21.46%, 30.86%, 8.88%, 13.69%, 31.41%, and 37.34%, respectively. The enhancement is more with INC compared to that of RBF, as the INC algorithm gets stuck at LMPP without reconfiguration and tracks the suboptimal output resulting in tracking the misleading power.

Hence, the proposed novel RBF integrated-intelligent reconfiguration strategy proved to be an efficient solution in mitigating the drawbacks of partial shading.

6 | FUTURE SCOPE

The proposed hybrid static reconfiguration-MPPT methodology can be further investigated for solar rooftop residential setups, commercial, and large-scale PV installations. In the future, the dynamic array reconfiguration strategies can also be integrated with the conventional and advanced MPPT strategies for maximizing and effectually tracking the GMP.

CONFLICT OF INTEREST STATEMENT

The authors report there are no competing interests to declare.

DATA AVAILABILITY STATEMENT

Data sharing is not applicable to this article as no new data were created or analyzed in this study.

ORCID

Chepuri Venkateswara Rao https://orcid.org/0000-0003-0938-4867
Rayappa David Amar Raj https://orcid.org/0000-0002-5888-5513

REFERENCES

1. Naik KA, Raj RDA, Rao CV, Babu TS. Generalized cryptographic image processing approaches using integer-series transformation for solar power optimization under partial shading. *Energ Conver Manage*. 2022;272:116376. doi:10.1016/j.enconman.2022.116376
2. Amar Raj RD, Naik KA. A novel solar photovoltaic array reconfiguration technique using two-dimensional generalized Arnold's cat map. *ASME J sol Energy Eng*. 2022;144(6):061001.
3. Raj RDA, Naik KA. A novel scan pattern for reconfiguration of partially shaded photovoltaic arrays for maximum power extraction. *Int J Circuit Theory Appl*. 2022;51:668-701.
4. Chellakhi A, El Beid S, Abouelmahjoub Y, Mchaouar Y. Optimization of power extracting from photovoltaic systems based on a novel adaptable step INC MPPT approach. *IFAC-PapersOnLine*. 2022;55(12):508-513.
5. Nassef M, Houssein EH, Helmy BE, Rezk H. Modified honey badger algorithm based global MPPT for triple-junction solar photovoltaic system under partial shading condition and global optimization. *Energy*. 2022;254(A):124363. doi:10.1016/j.energy.2022.124363
6. Deboucha H, Shams I, Belaid SL, Mekhilef S. A fast GMPPT scheme based on collaborative swarm algorithm for partially shaded photovoltaic system. *IEEE J Emerg Select Topics Power Electron*. 2021;9(5):5571-5580. doi:10.1109/JESTPE.2021.3071732
7. Deboucha H, Mekhilef S, Belaidand SL, Guichi A. Modified deterministic Jaya (DM-Jaya)-based MPPT algorithm under partially shaded conditions for PV system. *IET Power Electron*. 2021;13(19):4625-4632.
8. Houssein EH, Mahdy MA, Fathy A, Rezk H. A modified marine predator algorithm based on opposition based learning for tracking the global MPP of shaded PV system. *Expert Syst Appl*. 2021;183:115253. doi:10.1016/j.eswa.2021.115253
9. Makhloufi S, Mekhilef S. Logarithmic PSO-based global/local maximum power point tracker for partially shaded photovoltaic systems. *IEEE J Emerg Select Topics Power Electron*. 2022;10(1):375-386. doi:10.1109/JESTPE.2021.3073058
10. Zhao Z, Zhang M, Zhang Z, et al. Hierarchical pigeon-inspired optimization-based MPPT method for photovoltaic systems under complex partial shading conditions. *IEEE Trans Ind Electron*. 2022;69(10):10129-10143.
11. Balaji V, Fathima AP. Hybrid algorithm for MPPT tracking using a single current sensor for partially shaded PV systems. *Sustain Energy Technol Assess*. 2022;53(A):102415. doi:10.1016/j.seta.2022.102415
12. Ali ZM, Alquthami T, Alkhalaf S, Norouzi H, Dadfar S, Suzuki K. Novel hybrid improved bat algorithm and fuzzy system based MPPT for photovoltaic under variable atmospheric conditions. *Sustain Energy Technol Assess*. 2022;52(B):102156. doi:10.1016/j.seta.2022.102156
13. Hai T, Zhou J, Muranaka K. An efficient fuzzy-logic based MPPT controller for grid-connected PV systems by farmland fertility optimization algorithm. *Optik*. 2022;267:169636.
14. Sutikno T, Subrata AC, Elkhateb A. Evaluation of fuzzy membership function effects for maximum power point tracking technique of photovoltaic system. *IEEE Access*. 2021;9:109157-109165.
15. Fathi M, Parian JA. Intelligent MPPT for photovoltaic panels using a novel fuzzy logic and artificial neural networks based on evolutionary algorithms. *Energy Rep*. 2021;7:1338-1348. doi:10.1016/j.egyr.2021.02.051
16. Allahabadi S, Iman-Eini H, Farhangi S. Fast artificial neural network based method for estimation of the global maximum power point in photovoltaic systems. *IEEE Trans Ind Electron*. 2022;69(6):5879-5888.
17. Raj RDA, Naik KA. Optimal reconfiguration of PV array based on digital image encryption algorithm: a comprehensive simulation and experimental investigation. *Energ Conver Manage*. 2022;261:115666. doi:10.1016/j.enconman.2022.115666
18. Yang B, Ye H, Wang J, et al. PV arrays reconfiguration for partial shading mitigation: recent advances, challenges and perspectives. *Energ Conver Manage*. 2021;247:114738. doi:10.1016/j.enconman.2021.114738
19. Aljafari B, Satpathy PR, Thanikanti SB. Partial shading mitigation in PV arrays through dragonfly algorithm based dynamic reconfiguration. *Energy*. 2022;257:124795. doi:10.1016/j.energy.2022.124795
20. Zhang X, Yu T, Ma X, Guo L. An efficient multi-agent negotiation algorithm for multi-period photovoltaic array reconfiguration with a hydrogen energy storage system. *Energ Conver Manage*. 2022;256:115376. doi:10.1016/j.enconman.2022.115376
21. Ajmal AM, Ramachandaramurthy VK, Naderipour A, Ekanayake JB. Comparative analysis of two-step GA-based PV array reconfiguration technique and other reconfiguration techniques. *Energ Conver Manage*. 2021;230:113806. doi:10.1016/j.enconman.2020.113806
22. Alanazi M, Fathy A, Yousri D, Rezk H. Optimal reconfiguration of shaded PV based system using African vultures optimization approach. *Alex Eng J*. 2022;61(12):12159-12185. doi:10.1016/j.aej.2022.06.009
23. Quesada GV, Gispert FG, Lopez RP, Lumbreras MR, Roca AC. Electrical PV Array reconfiguration strategy for energy extraction improvement in grid-connected PV systems. *IEEE Trans Ind Electron*. 2009;56(11):4319-4331.
24. Parlak Ş. PV array reconfiguration method under partial shading conditions. *Int J Elec Power Energy Syst*. 2014;63:713-721. doi:10.1016/j.ijepes.2014.06.042
25. Cisneros HIS, Camacho PYS, Ocampo JBR, et al. A dynamic reconfiguration method based on neuro-fuzzy control algorithm for partially shaded PV arrays. *Sustain Energy Technol Assess*. 2022;52(B):102147. doi:10.1016/j.seta.2022.102147
26. Karakose M, Baygin M, Murat K, Baygin N, Akin E. Fuzzy based reconfiguration method using intelligent partial shadow detection in PV arrays. *Int J Comput Intell Syst*. 2016;9(2):202-212. doi:10.1080/18756891.2016.1150004

27. Nguyen D, Lehman B. An adaptive solar photovoltaic Array using model-based reconfiguration algorithm. *IEEE Trans Ind Electron*. 2008;55(7):2644-2654.
28. Anjum S, Mukherjee V, Mehta G. Modelling and simulation of AdDoKu based reconfiguration technique to harvest maximum power from photovoltaic array under partial shading conditions. *Simul Model Pract Theory*. 2022;115:102447. doi:10.1016/j.simpat.2021.102447
29. Tatabhatla VMR, Agarwal A, Kanumuri T. A chaos map based reconfiguration of solar array to mitigate the effects of partial shading. *IEEE Trans Energy Convers*. 2022;37(2):811-823.
30. Pachauri RK, Thanikanti SB, Bai J, et al. Ancient Chinese magic square-based PV array reconfiguration methodology to reduce power loss under partial shading conditions. *Energ Conver Manage*. 2022;253:115148. doi:10.1016/j.enconman.2021.115148
31. Yousri D, Fathy A, El-Saadany EF. Four square sudoku approach for alleviating shading effect on total-cross-tied PV array. *Energ Conver Manage*. 2022;269:116105. doi:10.1016/j.enconman.2022.116105
32. Reddy SS, Yammani C. Odd-even-prime pattern for PV array to increase power output under partial shading conditions. *Energy*. 2020; 213:118780. doi:10.1016/j.energy.2020.118780
33. Dhanalakshmi B, Rajasekar N. Dominance square based array reconfiguration scheme for power loss reduction in solar photovoltaic (PV) systems. *Energ Conver Manage*. 2018;156:84-102. doi:10.1016/j.enconman.2017.10.080
34. Raj A, David R, Naik KA. An image encryption concept based solar photovoltaic array reconfiguration techniques for mismatch mitigation. *Energy Sources A: Recovery Util Environ Eff*. 2022;44(1):951-972.
35. Amar Raj RD, Anil Naik K. A generalized henon map-based solar PV array reconfiguration technique for power augmentation and mismatch mitigation. *IETE J Res*. 2022;1-19.
36. Raj RDA, Aditya T, Shinde MR. Power quality enhancement of grid-connected solar photovoltaic system using LCL filter. In: *2020 International Conf. on Power Electronics & IoT Applications in Renew. Energy and its Control (PARC)*. Vol.2020. IEEE:334-339.
37. Ali MN, Mahmoud K, Lehtonen M, Darwish MMF. An efficient fuzzy-logic based variable-step incremental conductance MPPT method for grid-connected PV systems. *IEEE Access*. 2021;9:26420-26430.
38. Nuño JC, Muñoz FJ. "On the ubiquity of the ruler sequence." arXiv preprint arXiv:2009.14629,2020.
39. van de Bult, F.J., Gijswijt, D.C., Linderman, J.P., Sloane, N.J.A. and Wilks, A.R. (2006). A slow-growing sequence defined by an unusual recurrence. arXiv preprint math/0602498.
40. Puteaux P, Puech W. CFB-then-ECB mode-based image encryption for an efficient correction of noisy encrypted images. *IEEE Trans Circuits Syst Video Technol*. 2021;31(9):3338-3351.
41. Dong W, Li Q, Tang Y, Hu M, Zeng R. A robust and multi chaotic DNA image encryption with pixel-value pseudorandom substitution scheme. *Opt Commun*. 2021;499:127211. doi:10.1016/j.optcom.2021.127211
42. Zhang R, Li Y, Gui Y, Zhou J. Prediction of blasting induced air-overpressure using a radial basis function network with an additional hidden layer. *Appl Soft Comput*. 2022;127:109343. doi:10.1016/j.asoc.2022.109343
43. Zhang G, Luo J, Xu H, et al. An improved UKF algorithm for extracting weak signals based on RBF neural network. *IEEE Trans Instrum Meas*. 2022;71:1-14.
44. Bugshan N, Khalil I, Moustafa N, Almashor M, Abuadbba A. Radial basis function network with differential privacy. *Future Gener Comput Syst*. 2022;127:473-486.

How to cite this article: Rao CV, Raj RDA, Anil Naik K. A novel hybrid image processing-based reconfiguration with RBF neural network MPPT approach for improving global maximum power and effective tracking of PV system. *Int J Circ Theor Appl*. 2023;51(9):4397-4426. doi:10.1002/cta.3629

APPENDIX A

TABLE A1 Specifications of the overall PV system.

Component	Parameter	Symbol	Rating
Kyocera KC200GT PV panel	Power at GMP	P_{GMP}	200.14 W
	Open circuit voltage	V_{oc}	32.9 V
	Short circuit current	I_{sc}	8.21A
	Voltage at GMP	V_{GMP}	26.3 V
	Current at GMP	I_{GMP}	7.61 A
Boost converter	Switching frequency	f_{sw}	5000 Hz
	Load resistance	R_{Load}	12.847 Ω
	Capacitor	C_b	875 μF
	Inductor	L_b	5.6 mH
	DC link capacitor	C_{dc}	50 μF
Load resistance	Resistance	R_{Load}	12.847 Ω

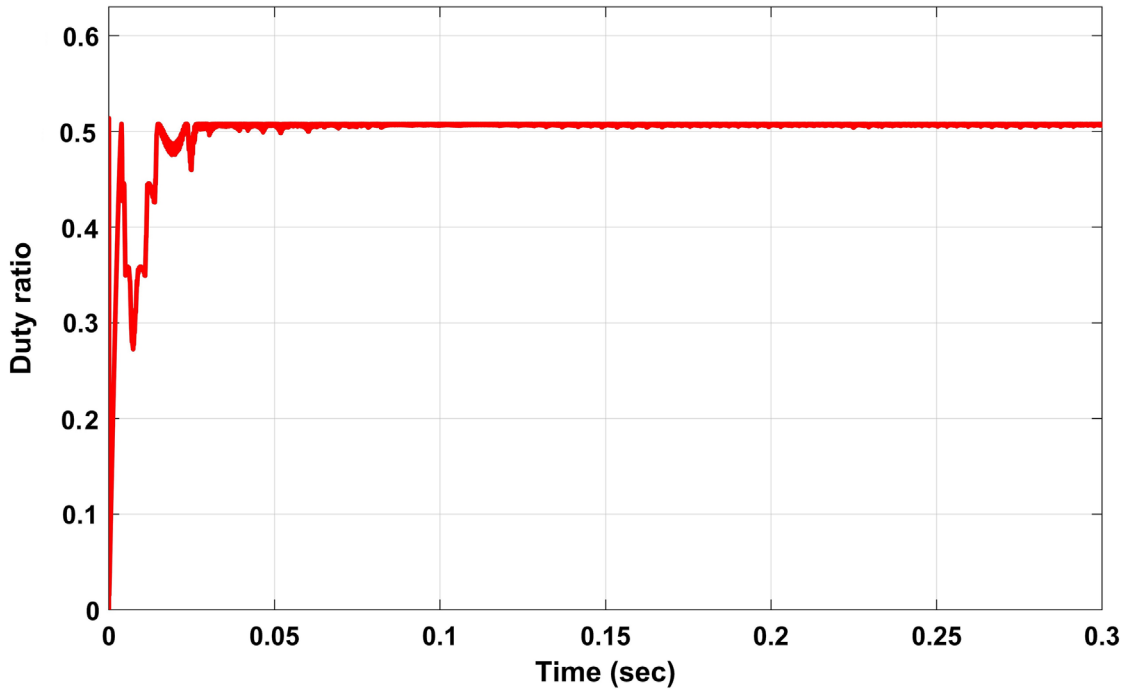

FIGURE A1 RBFNN-MPPT controller output curve.